Mon. Not. R. Astron. Soc. **000**, 1–25 (XXXX) Printed 20 July 2010 (MN LATEX style file v2.2)

The 6-GHz methanol multibeam maser catalogue II: Galactic longitudes 6° to 20°

J. A. Green,[1⋆] J. L. Caswell,[1] G. A. Fuller,[2] A. Avison,[2] S. L. Breen,[3,1] S. P. Ellingsen,[3] M. D. Gray,[2] M. Pestalozzi,[5] L. Quinn,[2] M. A. Thompson,[4] M. A. Voronkov[1]

[1] *CSIRO Astronomy and Space Science, Australia Telescope National Facility, PO Box 76, Epping, NSW 2121, Australia;*
[2] *Jodrell Bank Centre for Astrophysics, Alan Turing Building, School of Physics and Astronomy, University of Manchester, Manchester, M13 9PL, UK;*
[3] *School of Mathematics and Physics, University of Tasmania, Private Bag 37, Hobart, TAS 7001, Australia;*
[4] *Centre for Astrophysics Research, Science and Technology Research Institute, University of Hertfordshire, College Lane, Hatfield, AL10 9AB, UK;*
[5] *INAF/IFSI, via del Fosso del Cabaliere 100, I-00133, Roma*

Accepted 2010 July 15. Received 2010 July 13; in original form 2010 May 6

ABSTRACT

We present the second portion of an unbiased survey of the Galactic plane for 6668-MHz methanol masers. This section of the survey spans the longitude range 6° to 20°. We report the detection of 119 maser sources, of which 42 are new discoveries. The masers are tightly constrained to the Galactic plane, with only four outside a latitude range of ±1°. This longitude region includes the brightest known 6668-MHz methanol maser, 9.621+0.196, as well as the two brightest newly discovered sources in the southern survey as a whole. We list all the sources associated with the 3-kpc arms within ±15° longitude and consider further candidates beyond 15° longitude. We identify three new sources associated with the Galactic bar and comment on the density of masers in relation to the bar orientation.

Key words: masers − surveys − stars: formation − ISM: molecules.

1 INTRODUCTION

The Methanol Multibeam (MMB) survey is a project to survey the entire Galactic plane for 6668-MHz methanol masers (Green et al. 2009a). This species of maser is one of the brightest observed, it is widespread throughout the Galaxy, and it exclusively traces high-mass stars in an early stage of their formation (Pestalozzi et al. 2002; Minier et al. 2003; Xu et al. 2008). This makes the 6668-MHz methanol maser a powerful tool for understanding the processes of high-mass star formation and studying the spiral arm structure of our Galaxy (e.g. Reid et al. 2009; Rygl et al. 2010). By surveying in an unbiased manner, with uniform sensitivity, the MMB will establish a definitive catalogue for future studies. More than 60% of the Galactic plane has now been observed with the Parkes Radio Telescope and detections followed up to yield accurate positions (⩽0.4 arcsec). The catalogue is being released sequentially, as data reduction and follow-up observations are completed. The first region to be released covered Galactic longitudes 345° to 6° (Caswell et al. 2010), with a focus on recognising masers associated with the Galactic centre. The current paper extends the Galactic centre region to a longitude of 20°, and represents the remaining sources north of the Galactic centre which have high resolution positions from the Australia Telescope Compact Array (ATCA). For sources further north we are obtaining positions with the Multi-Element Radio Linked Interferometer Network (MERLIN) and the Very Large Array (VLA) and these will be presented in a subsequent paper.

A number of targeted searches have previously been made in the 6° to 20° longitude region presented here, with the targets consisting of masers of other methanol transitions and other molecular species (e.g. 12-GHz methanol and 1665/1667-MHz hydroxyl masers), as well as various star formation indicators (e.g. IRAS colour selected ultra-compact HII regions). The targeted observations include the first search for methanol at 6668-MHz (Menten 1991) that led to the discovery of maser emission in this transition. The other major targeted observations preceding the MMB survey were: Schutte et al. (1993); van der Walt et al.

⋆ E-mail:james.green@csiro.au

(1995); Caswell et al. (1995a); Walsh et al. (1997, 1998); Slysh et al. (1999); Szymczak et al. (2000); Beuther et al. (2002). The combination of these observations resulted in 74 sources known in this region prior to the MMB survey (Pestalozzi et al. 2005). The positions for 45 of these were presented in Caswell (2009). During the course of the survey three more sources have been detected (Ellingsen 2007 and Cyganowski et al. 2009).

Of special interest, this survey region includes the remaining sources regarded by Green et al. (2009b) as a likely population associated with the enigmatic 3-kpc arms (van Woerden et al. 1957; Oort et al. 1958; Bania 1977, 1980; Lockman 1980). The presence of 6668-MHz methanol masers in this interior Galactic feature conclusively demonstrated the presence of high-mass star formation, in both the well known near-side portion, and the recently discovered far-side portion (Dame & Thaddeus 2008). Understanding the nature and structure of this part of the Milky Way is key to understanding the structure and dynamics of the inner Galaxy.

2 METHANOL MULTIBEAM SURVEY PARAMETERS AND EQUIPMENT

A full review of the survey techniques is given in Green et al. (2009a), so only a brief description is presented here together with details specific to the 6° to 20° longitude region. The survey has been conducted with a purpose-built 7-beam receiver on the Parkes radio telescope together with subsequent ATCA observations (in the 6-km configurations) to provide high resolution positions (positional accuracy of ∼0.4 arcsec). At Parkes, blocks of the Galactic plane 2° in longitude by 4° in latitude were initially raster scanned. Maser sources in the resulting data cubes were first identified using an automated routine and then visually inspected. Once the high resolution positions were determined with the ATCA, seven-minute pointed Parkes observations, referred to as MX observations, were subsequently obtained towards the maser sources (including two sources known to exist outside the MMB latitude range). The Parkes beamwidth at 6668-MHz is 3.2 arcmin and the typical 1 σ noise level in the survey cubes was 0.17 Jy. The MX observations typically reached noise levels of 0.07 Jy. The spectral resolution at Parkes was 0.11 km s^{-1}. The latitude range of the MMB was ±2°, which was adequate for this region of the Galactic plane, because only four sources are known to exist outside ±1° and only two of these lie more than 2° from the plane.

The survey cubes for 6° to 14° longitude were observed over the period 2006 April to 2007 August, whereas 14° to 20° longitude were observed solely in 2007 August. Twelve of the 32 scans in the 8° to 10° longitude region were repeated in 2007 November due to higher than average noise in the originals. The MX observations for the 6° to 20° longitude region were taken in 2008 March, 2008 August and 2009 March.

As detailed in Green et al. (2009a), the velocity coverage was designed to cover all the known CO emission of Dame et al. (2001), with multiple velocity settings where needed (single setting coverage was ∼180 km s^{-1}). For the longitude range covered in this paper, two central velocity settings were required: between 6° and 10° these were centred at +135 km s^{-1} and −10 km s^{-1}; and between 10° and 20° they were centred at +145 km s^{-1} and 0 km s^{-1}.

3 SURVEY RESULTS

Results are presented in Table 1: column one is the source name (Galactic longitude and latitude); columns two and three are Right Ascension and Declination in J2000 coordinates from ATCA observations; columns four and five are the minimum and maximum velocities of emission (the most extreme values observed in any observations); columns six and seven are the MX peak velocities and flux densities; columns eight and nine are the peak velocities and flux densities observed in the survey cubes; and the final column provides extra information on the date of the ATCA observation (if it was observed by us) or a reference for comparable observations made previously. All velocities are with respect to the radio convention of the local standard of rest (LSR). For sources in close proximity, individual source velocity ranges have been determined from inspection of the higher spatial resolution ATCA data. Parkes spectra for the sources are given in Figure 1. These are all MX spectra with the exception of 14.230-0.509, which is the survey cube spectrum (the source is variable and was not detectable in the MX observations as discussed in Section 3.1). Typical physical sizes (⩽0.03 pc) and distances (⩾3 kpc) are such that maser spots associated with an individual exciting star (or binary) are spread over a diameter of less than 2 arcsec (Caswell 1997); as such we treat emission features separated by ⩾2 arcsec as different maser sites (Caswell 2009; Caswell et al. 2010). All our sources are separated by at least 10 arcsec, with the exception of the two pairs 18.733-0.224 with 18.735-0.227, and 19.472+0.170 with 19.472+0.170n. For completeness, we list the two additional sources known to exist outside the latitude range of the MMB survey (Pestalozzi et al. 2005) and give measurements from our targeted MX observations.

For the 6° to 20° longitude region we detected 119 sources, corresponding to an average of 8 sources per degree of longitude, with 42 new detections.

3.1 Remarks on sites of maser emission.

Here we provide additional details on notable sources and sources with confused spectral structure. This includes: 11 sources which are associated with the 3-kpc arms (Green et al. 2009b); 4 sources with relatively large latitudes; 6 with known variability; and 3 with velocity ranges wider than 16 km s^{-1}. The majority of sources within longitudes 6° to 20° are located within the solar circle (inferred from their positive LSR velocities) and therefore have a near-far ambiguity for kinematic distance estimates. Where possible we remark on sources which have been allocated a near or far distance in the literature.

6.189-0.358 This is the brightest (229 Jy) new detection of the MMB survey and is associated with the near 3-kpc arm.

6.368-0.052, 7.601-0.139 and 7.632-0.109 These three new sources all have high velocities (144.1 km s^{-1},

154.7 km s^{-1} and 157.0 km s^{-1} respectively) and are potentially associated with the Galactic bar. For the closely spaced pair, 7.601-0.139 incorporates the features between 155 and 157 km s^{-1}, whilst 7.632-0.109 incorporates the features outside these velocities. All three sources may be linked to the known high velocity HI at these longitudes, which extends from the plane to high latitudes (see for example McClure-Griffiths et al. 2005). 6.368-0.052 displays a feature of 0.2 Jy at 136 km s^{-1} in both the MX taken 2008 March and the MX taken 2009 March, however it has not been confirmed with the ATCA.

6.539-0.108, 6.588-0.192 and 6.610-0.082 We have detected a new source amongst two previously known sources. The new source, 6.588-0.192, has three blended peaks between 4 and 6 km s^{-1}. 6.539-0.108 has a clear feature at 13.5 km s^{-1} and 6.610-0.082 has a clear feature at 0.8 km s^{-1}, both known from previous observations. Additionally we detect weak emission between 6 and 7 km s^{-1} in the spectrum of 6.539-0.108 and weak emission (<0.9 Jy) at 5-6 km s^{-1} and ∼10 km s^{-1} in the spectrum of 6.610-0.082. The features in both spectra near 6 km s^{-1} may partially be a sidelobe response of the new source 6.588-0.192. A fourth source may exist in the region, but it could not be resolved with the ATCA, and would require future VLBI observations. LSR velocities near zero at this Galactic longitude imply heliocentric distances of either a few kpc or beyond 10 kpc. Downes et al. (1980) ascribe the associated HII region 6.553-0.095 to the far kinematic distance based on formaldehyde absorption. They also speculated that it might be in the 3-kpc arm, but this seems unlikely since the velocities do not correspond with either of the arms as defined in Dame & Thaddeus (2008).

6.795-0.257 This source has a wide velocity range of 19.3 km s^{-1} with the features between 25 km s^{-1} and 30 km s^{-1} probably separated from the bright feature at ∼14 km s^{-1} by approximately one arcsecond. Overall the features increased in flux density between the survey cube observation and the MX (2009 March).

7.166+0.131 This is a new source to the survey and clearly associated with the far 3-kpc arm. It also exhibits a wide velocity range of 16.5 km s^{-1}.

8.139+0.226 This source, when first discovered by Schutte et al. (1993), had a peak flux density of ∼15 Jy. A position was obtained in 2000 by Caswell (2009) with a peak flux density of only 3.5 Jy. The survey cube spectrum (taken 2006/2007) showed a higher peak flux density of 5.2 Jy. The MX taken in 2009 showed a peak flux density of over twice this at 11.4 Jy. On the basis of a lack of formaldehyde absorption, Wink et al. (1982) suggest the associated compact HII region is most likely at the near kinematic distance.

8.669-0.356 and 8.683-0.368 The spectra of this close pair of sources contain a feature at ∼36 km s^{-1} which is likely to be variable and could not be clearly attributed to either one of the sources. 8.669-0.356 comprises only the small feature at ∼39 km s^{-1}, whilst 8.683-0.368 contains all other features seen in the spectrum. Downes et al. (1980) ascribe the associated HII region to the near kinematic distance based on a lack of formaldehyde absorption.

8.832-0.028 This is a bright new source (159 Jy) also recently positioned by Xu et al. (2009) with the ATCA. It is associated with the near 3-kpc arm.

8.872-0.493 This new source was also recently positioned by Xu et al. (2009) with the ATCA. It is potentially associated with the molecular cloud 8.9-0.5 (velocity of 12 km s^{-1}) from Solomon et al. (1987), which was claimed by the authors to have kinematics matching those of the near 3-kpc arm. However, the kinematics do not match an extrapolation of the arm based on Cohen & Davies (1976) nor the more recent definition of Dame & Thaddeus (2008). Applying current kinematic models, the velocity of 8.872-0.028 (∼23 km s^{-1}) would place it in either the Carina-Sagittarius or Perseus arms. If the maser is associated with the 8.9-0.5 molecular cloud (with a 10 km s^{-1} unusual velocity), then that would place it more likely in the Perseus, rather than the Carina-Sagittarius arm. In either case the source is unlikely to be associated with the near 3-kpc arm.

9.621+0.196 and 9.619+0.193 This famous source and its companion have been extensively studied since discovery in 1991 (Menten 1991; Norris et al. 1993; Walsh et al. 1997, 1998; Phillips et al. 1998; Caswell 2009). There has also been extensive monitoring of 9.621+0.196 by Caswell et al. (1995b); Goedhart et al. (2003, 2004); van der Walt et al. (2009); Vlemmings et al. (2009), with Goedhart et al. (2003) detecting periodic flares (see Section 4.3 for details). The weaker source, 9.619+0.193, probably has just two features. Several authors have postulated the pair lie within the 3-kpc arm (e.g. Caswell et al. 1995a; Hofner et al. 1994; Green et al. 2009b) and recent trigonometric parallax measurements of 12 GHz methanol (Sanna et al. 2009) established a heliocentric distance of 5.2±0.6 kpc (corresponding to a Galactocentric distance consistent with 3-kpc arm estimates).

9.986-0.028 This source consists of a group of three strong (>10 Jy) features between 40 km s^{-1} and 45 km s^{-1} (two of which are blended in the Parkes spectrum), an outlying strong feature at 47 km s^{-1} and other weaker (<10 Jy) emission between 40 km s^{-1} and 52 km s^{-1}. The 47 km s^{-1} feature was the brightest at 35 Jy in the original Schutte et al. (1993) Hartebeesthoek observations, but had decreased to 28 Jy in the ATCA observations made in 2000 by Caswell (2009). In our observations this feature is stable between the survey cube (2007 January) and MX (2009 March) observations with a peak flux density of ∼27 Jy. Meanwhile the feature at 42 km s^{-1} which had shown a steady increase from ∼15 Jy to 26 Jy between the Schutte et al. (1993) and Caswell (2009) observations now dominates the spectrum. Our survey cube and MX observations find a peak flux density of ∼70 Jy. The 43.5 km s^{-1} feature decreased from 32 Jy in 1993 to 20 Jy in 2000, increased to 24 Jy in the survey cube and decreased to 20 Jy in the MX. The 40.5 km s^{-1} feature has been stable at ∼25 Jy across all the observations with the exception of the survey cube where it flared to 38 Jy.

10.205-0.345, 10.287-0.125, 10.299-0.146, 10.323-0.160 and 10.342-0.142 These are the first of four groups of sources which are in the direction of the W31 complex. The close proximity of all these sources leads to confusion in the Parkes spectra, however the high spatial resolution of the ATCA observations allows identification of the different source features: 10.205-0.345 has emission between 5 and 11 km s^{-1} with a peak at 7.2 km s^{-1}; 10.287-0.125 contains the three features with velocities less than 5 km s^{-1}; 10.299-0.146 is the small feature at ∼20 km s^{-1}; 10.323-0.160 is the feature at 6 km s^{-1} and the double feature between 9 and 13 km s^{-1}; 10.342-0.142 exists between 7 and 17 km s^{-1}, but not including the bright peaks of the previous mentioned source. 10.323-0.160 has been monitored for variability by Goedhart et al. (2004). 10.287-0.125 and 10.342-0.142 are associated with Extended Green Objects (Cyganowski et al. 2009). Wilson et al. (1984) detected methanol absorption at 23 GHz.

10.320-0.160 and 10.356-0.148 These sources, also in the direction of W31, have emission at higher velocities: 10.320-0.160 comprises the features between 35 and 40 km s^{-1}; 10.356-0.148 the features between between 49 and 54 km s^{-1}.

10.444-0.018, 10.472+0.027 and 10.480+0.033 Although close to W31 spatially, the high velocities of this trio of sources separates them from the complex. 10.472+0.027 and 10.480+0.033, separated by ∼6 arcmin, and originally identified as 10.47+0.03, were highlighted by Caswell et al. (1995b) as extremely variable and have been monitored for variability by Goedhart et al. (2004). The sources have a very wide range of velocity emission which is comparable to the nearby source 10.444-0.018.

10.627-0.384 and 10.629-0.333 This is the fourth group of sources which have been loosely associated with W31. 10.627-0.384 includes the small feature on the edge of the absorption at approximately -6 km s^{-1}, but not the outlying features. Absorption was also evident in the Parkes spectrum shown by Caswell et al. (1995a). 10.629-0.333 is kinematically associated with the near 3-kpc arm as defined by Dame & Thaddeus (2008). Although marginally offset in peak velocity, the close spatial association of 10.627-0.384 together with its emission at negative velocities, implies this source is also associated. The other 3 groups of sources previously mentioned are offset in position and velocity from 10.627-0.384 and 10.629-0.333, so do not appear to be associated with the near 3-kpc arm as defined by Dame & Thaddeus (2008). This implies that 10.629-0.333 and 10.627-0.384 may be a chance spatial alignment with W31 and not actually associated. Conversely if the whole W31 complex is associated with the near 3-kpc arm, as was suggested by Downes et al. (1980), the 3-kpc arm kinematics differ from that observed by Dame & Thaddeus (2008). Fish et al. (2003) argues that 10.629-0.333 is unlikely to be at the far distance based on HI absorption observations towards an associated compact HII region.

10.724-0.334 This source is associated with the near 3-kpc arm. It has significantly brightened from 1.5 Jy in the survey cube observation to 5 Jy in the MX.

10.822-0.103 This source had three features in the survey cube observation, between 68 km s^{-1} and 74 km s^{-1}. The ATCA data detected all three, but at minimal signal-to-noise. The MX taken 2009 March only detected one feature at a velocity of 69 km s^{-1}.

10.886+0.123 Both the survey cube and MX data (2008 March) show consistency in the shape of the spectrum and the peak flux densities of the features, although the ATCA spectrum had flux densities a factor of two lower.

11.034+0.062 The 25 km s^{-1} feature seen in the spectrum is a sidelobe response to 10.958+0.022.

11.109-0.114 This new source to the survey was also detected by Ellingsen (2007), but listed as 11.15-0.14.

11.903-0.102 and 11.904-0.141 Of this pair of sources 11.904-0.141 accounts for the features between ∼40 and 45 km s^{-1} and 11.903-0.102 for the lower velocity features. No variability was present between the observations of Caswell et al. (1995a) and Caswell (1997), however our observations find that for 11.903-0.102 the original peak feature at 36 km s^{-1} has increased from 1.8 Jy (Caswell 1997) to 4.5 Jy. Additionally the feature at 33.8 km s^{-1} has increased from 1.5 Jy (Caswell 1997) to ∼11.5 Jy.

11.936-0.150 This source only contains the features seen between 45 and 50 km s^{-1}. Features <45 km s^{-1} are side-lobe responses to 11.904-0.141.

11.936-0.616 This source is associated with an Extended Green Object (Cyganowski et al. 2009). Solomon et al. (1987) attribute the associated molecular cloud, 12.00-0.60, to the near kinematic distance based on a velocity-linewidth argument.

12.025-0.031 This is a known source clearly associated with the far 3-kpc arm.

12.181-0.123, 12.199-0.033, 12.202-0.120, 12.203-0.107 and 12.209-0.102 This complex cluster of 5 sources is divided as: 12.181-0.123 which consists of the two features at ∼30 km s^{-1}; 12.202-0.120 which comprises the features between 20 and ∼32.5 km s^{-1}; 12.203-0.107 which is the feature peaking at 20.5 km s^{-1}; 12.209-0.102 which is composed of the weak features between 15 and ∼23 km s^{-1}; 12.199-0.033, although spatially close, is well separated in velocity.

12.625-0.017 The brightest feature of this maser at 21.6 km s^{-1} has increased from ∼10 Jy (2007 August) to almost 25 Jy (2008 March).

12.681-0.182 This source has previously been seen to vary from maximum flux density to minimum flux density by a factor of 1.5 over a three month period (Caswell et al. 1995b) and was a source monitored for variability by Goedhart et al. (2004), who found that all maser peaks exhibited a simultaneous variation with a quasi-periodic timescale of 307±60 days. We made three observations, the original survey cube in 2007 August and two MX observations

taken 2008 March and 2009 March. The 2007 August and 2008 March spectra show consistent spectral features (with flux densities comparable to within 5%) with the exception of the two features at 59 and 60 km s^{-1}, which decreased by ∼20%. In the 2009 March spectrum the features at 57.5, 59 and 60 km s^{-1} had all decreased from the 2007 August flux densities by 12%, 60% and 46% respectively.

12.889+0.489 The features of this source were seen to vary from maximum flux density to minimum flux density by a factor of 1.3 over an eight month period (Caswell et al. 1995b) and it was then monitored for variability by Goedhart et al. (2004) and Goedhart et al. (2009). It has been shown to have a short period of only 29.5 days. The MMB survey cube observations have a peak flux density of 78.9 Jy (2007 August) and the MX 68.9 Jy (2008 March). See also Section 4.3.

12.909-0.260 This source is associated with W33 and has been monitored for variability by Goedhart et al. (2004). The authors found the 39.4 km s^{-1} and 39.8 km s^{-1} features showed little variation, whilst the 35.9 km s^{-1} feature had a monotonic increase from 12 to 20 Jy over their duration of their observations. We find a peak flux density of 245 Jy at 39.9 km s^{-1} in the survey cube rising to 269 Jy in the later MX (2008 March). Additional MX observations in 2009 March found 210 Jy (at 39.4 km s^{-1}) and 250 Jy (at 39.9 km s^{-1}). The feature at 35.9 km s^{-1} had a flux density of 25 Jy at the time of the survey cube, 22.5 Jy in 2008 March MX, and 22 Jy in 2009 March MX. The nearby object listed as 12.79-0.19 in Menten (1991) and not detected by either Caswell et al. (1995a) or Caswell (2009) was again not detected in a targeted MX observation. Clear absorption of ∼2 Jy was found in the Parkes spectrum, but no detectable spectral structure indicative of maser emission. In agreement with Voronkov et al. (2010), this location is about 7 arcmin from 12.909-0.260 and the 5 Jy peak flux density listed by Menten (1991) implies 12.79-0.19 was a sidelobe response to 12.909-0.260.

13.696-0.156 This is a new source detected by the MMB survey and is clearly associated with the far 3-kpc arm.

14.101+0.087 This source is associated with the near 3-kpc arm and a position was recently obtained by Xu et al. (2009).

14.230-0.509 This source was observed as a single feature peak of 3.6 Jy at 25.3 km s^{-1} in the survey cube observations. It was then undetectable in both the 2008 March MX and the ATCA observation taken in 2008 October. Fortunately it was detected again with the ATCA in 2009 January and a position was successfully obtained, with a peak flux density of 0.4 Jy at the original velocity of 25.3 km s^{-1}. It was then undetected in a subsequent MX taken 2009 March.

14.521+0.155 This is a new source associated with the near 3-kpc arm. A feature of 0.5 Jy at -2 km s^{-1} was seen in the MX observation (2009 March) which was not present in the prior survey cube observation.

14.991-0.121 This source includes two weak features at 52.5 km s^{-1} and 54 km s^{-1}.

15.034-0.677 This source is associated with the HII region in M17 (Caswell 1997). The brighter of the two features in this source was observed in the survey cubes to be stronger than any previous observations with a peak flux density of 51.6 Jy. The weaker of the two features has remained constant at ∼10 Jy.

15.607-0.255 This source was originally observed at 0.85 Jy, but faded to 0.4 Jy in an MX taken 2008 March and then was not detectable (<0.2 Jy) in the MX taken 2008 August. It was however detected again in 2008 October with the ATCA (with a peak flux density of 0.4 Jy).

16.302-0.196 The velocity range of emission is nominally 46.9 km s^{-1} to 53.6 km s^{-1}, but there is a weak spectral feature at ∼41 km s^{-1} in one MX, which was not seen in the original survey cube observation, or the ATCA observation.

16.585-0.051 The 59 km s^{-1} feature of this source was seen to be steadily decreasing in flux density over a period of 6 months by Caswell et al. (1995a). We find this feature is marginally weaker at 18 Jy (compared to ∼20 Jy in Caswell et al.). The feature at 64 km s^{-1} has remained stable at ∼15 Jy, but the 62 km s^{-1} feature has significantly increased from 18 Jy to 37 Jy. In the current observations we do not detect (<0.15 Jy) the two weak features at 52.8 km s^{-1} and 54.2 km s^{-1} seen by Caswell et al., instead finding a range of emission from 56.5 to 69.5 km s^{-1}. However for completeness we list the full velocity range in Table 1.

16.864-2.159 and 17.021-2.403 Both these sources lie outside the latitude range of the MMB survey, but were re-observed with MX observations for completeness. 16.864-2.159 was originally discovered by Caswell et al. (1995a) in a targeted search towards OH masers and has since been observed by Walsh et al. (1997, 1998) and Szymczak et al. (2000). Its spectrum has not changed over the >10 year period of these observations and our own. 17.021-2.403 was discovered by Szymczak et al. (2000) in a targeted search of IRAS sources and our observations expand the velocity range of the source with the detection of a weak (<1 Jy) feature at 18 km s^{-1}. The feature at 21 km s^{-1} has also increased significantly from the original observation of ∼1 Jy to 4 Jy.

16.976-0.005 This is a new weak source with a peak flux density of 0.7 Jy at 6.6 km s^{-1}.

17.638+0.157 This source was discovered in 1991 by MacLeod & Gaylard (1992) with a peak flux density of 25 Jy at 21 km s^{-1}. It was observed again in 1992 by Caswell et al. (1995a) with a flux density of 25 Jy and in 1999 by Szymczak et al. (2000) with a reduced flux density of 20 Jy. A position was determined with the ATCA in 2003 (Caswell 2009), finding a significantly further reduced flux density of 9.5 Jy. Our survey cube observations in 2007 August found an increase again with a peak flux density of 35 Jy. The MX in 2009 March recorded a peak flux density comparable to the original value of 25 Jy.

18.073+0.077 This source contains two bright features separated by approximately 6 km s^{-1}.

18.159+0.094 The relative intensity of the two strong features at 58 to 59 km s^{-1} has varied, with the 58.4 km s^{-1} feature remaining relatively constant at ∼8.5 Jy, but the feature at 59 km s^{-1} decreasing from 10.3 Jy in the survey cube (2007 August) to just shy of 2 Jy in the MX (2009 March). In addition to the major features, the MX detected a small feature (∼1 Jy) at 54.5 km s^{-1}, which was only marginally detected at 0.7 Jy in the survey cube and not detected in the ATCA observations.

18.440+0.045 This source has noticeable changes in its structure with the peak moving from ∼58 km s^{-1} (2007 August) to ∼62 km s^{-1} (2008 August) and a new feature appearing at ∼60 km s^{-1}. The feature at 49 km s^{-1} is a sidelobe of 18.460-0.004.

18.661+0.034 and 18.667+0.025 These are a closely spaced pair of sources, previously listed as one known site, but now distinguished as two sites. 18.661+0.034 extends to the higher velocities. 18.667+0.025 is mainly the features at 77 km s^{-1} and 80.5 km s^{-1} and is associated with an Extended Green Object (Cyganowski et al. 2009).

18.735-0.227 and 18.733-0.224 These sources are a closely spaced pair of new detections. The bright peak feature at 38 km s^{-1} belongs to 18.735-0.227, but the 3 other peaks are 18.733-0.224.

18.888-0.475 This new source was also recently detected by Cyganowski et al. (2009) associated with an Extended Green Object.

19.009-0.029 This new source was also recently detected by Ellingsen (2007), listed as 18.99-0.04. It was seen offset from a GLIMPSE source by 1.5 arcmin and is unlikely to be physically associated.

19.249+0.267 This source does not include the feature seen at 25 km s^{-1} which is a sidelobe of 19.365-0.030.

19.472+0.170n, 19.472+0.170 and 19.486+0.151 Two sources separated by less than 4 arcsec, are distinguished by an 'n' identifying the source with the more northerly declination (previously the southern site was instead identified with an 'sw' e.g. Caswell 2009, but we adopt an 'n' in accord with the Galactic centre region results of Caswell et al. 2010). The northern site contains the features at 18.5, 22 and 23 km s^{-1} the southern site, the features between 13 and 16 km s^{-1}. 19.486+0.151 comprises the other features at 20.5 km s^{-1}, 24 km s^{-1} and beyond to higher velocities.

19.609-0.234 This source consists of two main features, one at 36 km s^{-1} and one at 40 km s^{-1}. The 36 km s^{-1} feature had been the strongest feature, at 0.4 Jy, in the 1992 discovery spectrum (Caswell et al. 1995b). However this feature was a marginal detection in the survey cube data (2007 August). Fortunately the weak feature of 0.25 Jy at 40 km s^{-1} in 1992 flared to 1 Jy in the survey cube, allowing an ATCA position measurement in 2007 July (0.4 Jy peak). The 36 km s^{-1} feature rose to 0.5 Jy in an MX in March 2008, but was undetectable in an MX in March 2009. The 40 km s^{-1} feature had a peak flux density of 0.65 Jy in the MX measurement of 2009 March (and is shown in Figure 1). Kolpak et al. (2003); Anderson & Bania (2009); Roman-Duval et al. (2009) ascribe this source to a far kinematic distance based on an absence of HI self-absorption, whilst Downes et al. (1980) ascribe it to a near kinematic distance based on an absence of formaldehyde absorption.

19.612-0.120 and 19.612-0.134 As identified by Walsh et al. (1998), in addition to the main source 19.612-0.120 which has several features between 49 and 61 km s^{-1}, there is a narrow offset source peaking at 52-53 km s^{-1}. Both Kolpak et al. (2003) and Anderson & Bania (2009) ascribe the associated HII region to a far kinematic distance based on HI absorption and HI self-absorption, in contrast to Downes et al. (1980), who ascribe it to a near kinematic distance based on the absence of formaldehyde absorption.

19.667+0.114 This source peaked in emission at 16.3 km s^{-1} in the survey cube observation, but peaked at 14.2 km s^{-1} in the MX observation, with the 14 km s^{-1} feature doubling in strength from the MX observation from 1.1 Jy to 2.2 Jy. The features either side of the 16.3 km s^{-1} feature have also increased considerably in flux density (whilst the original 16.3 km s^{-1} feature has remained approximately the same).

19.884-0.534 This source has been identified as a far-side object from the presence of formaldehyde absorption (at a level of 7σ) by Sewilo et al. (2004). In contrast Roman-Duval et al. (2009) identify it as a near-side object based on the 'on-off' HI self absorption technique, as do Solomon et al. (1987) based on a line-width to distance relation.

4 DISCUSSION

Discussion of the global properties of the methanol maser population will be deferred until the full MMB catalogue is published. Here we discuss the properties of the sources within the 6° to 20° longitude region with reference to those in the Galactic centre region (Caswell et al. 2010).

4.1 Galactic Latitude distribution

The maser population in the 6° to 20° longitude region is confined to a narrow range of latitude (Fig. 2); 97% of the sources (115 out of 119 sources) are at a latitude within 1° of the Galactic plane. This narrow distribution is very similar to that seen in the 345° to 6° longitude region (Caswell et al. 2010). All four sources with latitudes outside 1° of the plane were previously known (11.497-1.485, 16.864-2.159, 17.021-2.403, 18.341+1.768).

4.2 Flux densities

The brightest 6668-MHz methanol maser detected to date, 9.621+0.196, is within the current region and was found

Table 1. Positions and parameters of methanol masers. The references are: W98: Walsh et al. (1998), B02: Beuther et al. (2002), X09: Xu et al. (2009), C2009: Caswell (2009). Position is from non-bracketed reference.

Source Name	Equatorial Coordinates		Velocity range		MX data		Survey Cube data		Position
(l, b)	RA(2000)	Dec(2000)	V_L	V_H	V_{pk}(MX)	S_{pk}(MX)	V_{pk}(SC)	S_{pk}(SC)	Refs, epoch
(° °)	(h m s)	(° ' ")	(km s^{-1})		(km s^{-1})	(Jy)	(km s^{-1})	(Jy)	
06.189−0.358	18 01 02.16	-23 47 10.8	-37.5	-27.1	-30.2	228.57	-30.2	221.60	2007JUL19
06.368−0.052	18 00 15.82	-23 28 43.8	141.0	147.8	144.1	1.50	144.1	1.49	2007JUL22
06.539−0.108	18 00 50.86	-23 21 29.8	12.7	13.8	13.1	0.60	13.4	0.50	C2009
06.588−0.192	18 01 16.09	-23 21 27.3	3.5	7.0	5.1	8.01	5.0	7.70	2007JUL21
06.610−0.082	18 00 54.03	-23 17 03.1	-6.6	7.5	0.8	23.40	0.8	21.20	C2009
06.795−0.257	18 01 57.75	-23 12 34.9	12.1	31.4	16.3	91.07	16.3	55.08	C2009
06.881+0.093	18 00 49.38	-22 57 42.6	-3.8	-1.5	-2.3	3.12	-2.1	3.25	2007JUL21
07.166+0.131	18 01 17.48	-22 41 44.0	74.5	91.0	85.7	2.58	85.7	2.47	2007JUL22
07.601−0.139	18 03 14.43	-22 27 00.9	151.0	156.5	154.6	8.69	154.7	8.12	2007JUL22
07.632−0.109	18 03 11.63	-22 24 32.4	146.5	158.9	157.0	6.55	157.0	6.26	2007JUL22
08.139+0.226	18 03 00.75	-21 48 09.9	18.8	21.8	19.9	11.40	19.9	5.24	C2009
08.317−0.096	18 04 36.02	-21 48 19.6	44.0	49.2	47.6	3.82	47.1	3.03	2007JUL21
08.669−0.356	18 06 18.99	-21 37 32.2	35.8	39.7	39.2	9.96	39.0	10.46	C2009
08.683−0.368	18 06 23.49	-21 37 10.2	35.8	45.6	43.2	102.00	43.2	141.70	C2009
08.832−0.028	18 05 25.67	-21 19 25.1	-6.0	5.9	-3.8	159.08	-3.8	126.80	2007MAR21; (X09)
08.872−0.493	18 07 15.34	-21 30 53.7	22.5	27.5	23.3	33.86	23.3	27.37	2007JUL21; (X09)
09.215−0.202	18 06 52.84	-21 04 27.5	36.0	50.0	45.5	11.96	45.6	9.16	2007JUL21
09.621+0.196	18 06 14.67	-20 31 32.4	-4.8	8.9	1.3	5239.85	1.3	5196.00	C2009
09.619+0.193	18 06 14.92	-20 31 44.3	5.0	7.0	5.5	70.00	5.4	65.00	C2009
09.986−0.028	18 07 50.12	-20 18 56.5	40.6	51.8	42.2	67.58	42.2	70.24	C2009
10.205−0.345	18 09 28.43	-20 16 42.5	5.6	11.0	6.6	2.03	7.2	1.28	2008OCT20
10.287−0.125	18 08 49.36	-20 05 59.0	1.5	6.0	4.6	7.19	4.5	8.29	C2009; (W98)
10.299−0.146	18 08 55.54	-20 05 57.5	19.0	21.0	19.9	0.94	20.0	1.51	C2009
10.320−0.259	18 09 23.30	-20 08 06.9	35.0	39.6	39.0	9.50	39.0	8.87	C2009
10.323−0.160	18 09 01.46	-20 05 07.8	4.0	16.0	11.5	90.05	11.6	94.62	C2009
10.342−0.142	18 08 59.99	-20 03 35.4	6.0	18.0	15.4	15.05	14.8	14.00	C2009
10.356−0.148	18 09 03.07	-20 03 02.2	49.6	54.2	49.9	1.45	50.0	1.20	2010MAY22
10.444−0.018	18 08 44.88	-19 54 38.2	67.6	79.0	73.3	24.27	73.4	24.92	C2009
10.472+0.027	18 08 38.20	-19 51 50.1	57.5	77.6	75.0	28.01	75.1	35.07	C2009
10.480+0.033	18 08 37.88	-19 51 16.1	57.0	66.0	59.5	22.53	59.5	24.07	C2009
10.627−0.384	18 10 29.22	-19 55 41.1	-6.0	7.7	4.6	4.23	4.6	3.78	C2009
10.629−0.333	18 10 17.98	-19 54 04.8	-13.5	1.0	-0.2	4.97	-0.4	4.20	C2009
10.724−0.334	18 10 30.03	-19 49 06.8	-2.5	-1.6	-2.2	4.78	-2.1	1.51	2007FEB05
10.822−0.103	18 09 50.52	-19 37 14.1	68.0	74.0	72.0	0.28	72.1	0.90	2007FEB06
10.886+0.123	18 09 07.98	-19 27 21.8	14.0	22.5	17.1	12.03	17.2	12.24	2007FEB06
10.958+0.022	18 09 39.32	-19 26 28.0	23.0	25.5	24.5	12.30	24.5	16.63	C2009
11.034+0.062	18 09 39.84	-19 21 20.3	15.2	21.0	20.5	0.55	20.6	0.89	C2009
11.109−0.114	18 10 28.25	-19 22 29.1	22.0	34.5	24.0	15.02	24.1	14.81	2007FEB05
11.497−1.485	18 16 22.13	-19 41 27.1	4.8	17.0	6.6	68.40	6.7	61.75	C2009
11.903−0.102	18 12 02.70	-18 40 24.7	32.0	36.7	33.9	11.30	33.8	11.60	C2009
11.904−0.141	18 12 11.44	-18 41 28.6	39.5	45.0	42.9	64.89	42.8	66.53	C2009
11.936−0.150	18 12 17.29	-18 40 02.6	46.0	50.0	48.5	2.15	48.4	2.30	C2009
11.936−0.616	18 14 00.89	-18 53 26.6	30.1	44.6	32.3	42.91	32.2	49.32	C2009
11.992−0.272	18 12 51.19	-18 40 38.4	56.0	60.5	59.8	1.89	59.8	1.60	2007FEB06; (W98)
12.025−0.031	18 12 01.86	-18 31 55.7	105.0	113.1	108.3	96.26	108.3	103.10	C2009
12.112−0.126	18 12 33.39	-18 30 07.6	38.0	52.0	39.9	2.98	39.9	2.80	2008JAN23
12.181−0.123	18 12 41.00	-18 26 21.9	29.0	31.0	29.7	1.92	29.7	1.40	C2009
12.199−0.033	18 12 23.44	-18 22 50.7	48.2	57.1	49.3	13.67	49.3	16.91	C2009; (2008JAN23)
12.202−0.120	18 12 42.93	-18 25 11.8	26.0	27.0	26.4	0.80	26.4	0.60	C2009
12.203−0.107	18 12 40.24	-18 24 47.5	20.0	32.0	20.5	2.43	20.5	1.83	C2009
12.209−0.102	18 12 39.92	-18 24 17.9	16.0	22.0	19.8	11.48	19.8	10.16	C2009
12.265−0.051	18 12 35.40	-18 19 52.3	58.0	70.9	68.5	2.25	68.3	2.56	C2009
12.526+0.016	18 12 52.04	-18 04 13.6	38.8	44.0	42.6	3.07	42.5	3.30	2008JAN23
12.625−0.017	18 13 11.30	-17 59 57.6	21.2	28.0	21.6	25.49	21.6	23.61	C2009; (B02)
12.681−0.182	18 13 54.75	-18 01 46.6	50.0	62.0	57.5	350.98	57.5	350.50	C2009
12.776+0.128	18 12 57.57	-17 47 49.2	30.4	33.0	32.8	0.84	32.9	0.90	2007NOV25
12.889+0.489	18 11 51.40	-17 31 29.6	28.0	43.0	39.3	68.88	39.2	78.93	C2009
12.904−0.031	18 13 48.27	-17 45 38.8	55.8	61.0	59.1	19.99	59.1	40.34	2008JAN23
12.909−0.260	18 14 39.53	-17 52 00.0	34.7	47.0	39.9	269.05	39.9	245.48	C2009

Table 1. Positions and parameters of methanol masers cont.

Source Name	Equatorial Coordinates		Velocity range		MX data		Survey Cube data		Position
(l, b)	RA(2000)	Dec(2000)	V_L	V_H	V_{pk}(MX)	S_{pk}(MX)	V_{pk}(SC)	S_{pk}(SC)	Refs, epoch
(° °)	(h m s)	(° ' ")	(km s^{-1})		(km s^{-1})	(Jy)	(km s^{-1})	(Jy)	
13.179+0.061	18 14 00.96	-17 28 32.5	45.6	50.0	46.5	1.48	46.5	2.57	2008JAN23
13.657−0.599	18 17 24.26	-17 22 12.5	45.0	52.7	51.2	32.22	51.3	33.71	C2009; (2008JAN23)
13.696−0.156	18 15 51.05	-17 07 29.6	98.3	108.5	99.3	1.90	99.4	1.86	2007NOV25
13.713−0.083	18 15 36.99	-17 04 31.8	43.0	53.2	43.6	12.74	43.6	12.63	2008JAN23; (2007NOV25)
14.101+0.087	18 15 45.81	-16 39 09.4	4.4	16.6	15.4	87.26	15.4	86.55	C2009
14.230−0.509	18 18 12.59	-16 49 22.8	24.6	26.7	25.3	0.20	25.3	3.62	2009JAN09; (2008OCT20)
14.390−0.020	18 16 43.77	-16 27 01.0	24.5	28.5	26.9	3.12	26.9	4.40	2008OCT20
14.457−0.143	18 17 18.79	-16 27 57.5	38.0	44.2	43.2	0.81	43.1	1.48	2008OCT20
14.490+0.014	18 16 48.06	-16 20 45.0	19.8	24.5	20.2	1.28	20.2	1.15	2008OCT20
14.521+0.155	18 16 20.73	-16 15 05.5	-3.0	6.0	4.1	1.40	4.1	1.31	2008OCT20
14.604+0.017	18 17 01.14	-16 14 38.0	22.1	35.8	24.6	2.33	24.7	2.30	2008AUG23; (W98)
14.631−0.577	18 19 15.21	-16 30 04.5	23.9	25.9	25.2	1.10	25.2	1.18	2008OCT20
14.991−0.121	18 18 17.32	-15 58 08.3	44.6	54.0	46.0	7.25	46.0	6.63	2008AUG23
15.034−0.677	18 20 24.78	-16 11 34.6	20.0	24.0	21.3	47.48	21.3	51.59	C2009
15.094+0.192	18 17 20.82	-15 43 46.5	22.5	26.5	25.7	13.63	25.8	18.62	2008AUG23
15.607−0.255	18 19 59.34	-15 29 22.8	65.1	66.5	65.9	0.43	66.0	0.85	2008OCT20
15.665−0.499	18 20 59.75	-15 33 10.0	-5.0	-2.0	-2.9	42.60	-2.9	47.65	2008AUG23
16.112−0.303	18 21 09.14	-15 04 00.6	33.4	35.6	34.5	2.05	34.5	2.22	2008AUG23
16.302−0.196	18 21 07.83	-14 50 54.6	46.9	53.6	51.9	11.24	51.8	9.91	2008AUG23
16.403−0.181	18 21 16.39	-14 45 09.0	39.1	40.0	39.2	0.47	39.2	0.50	2008OCT20
16.585−0.051	18 21 09.13	-14 31 48.5	52.0	69.5	62.1	36.74	62.1	33.30	2008AUG23; (W98)
16.662−0.331	18 22 19.46	-14 35 39.1	42.5	44.2	43.0	3.19	43.0	2.56	2008AUG23
16.831+0.079	18 21 09.53	-14 15 08.6	57.2	69.4	58.7	4.06	58.7	4.44	2008AUG23
16.855+0.641	18 19 09.57	-13 57 57.5	23.0	25.0	24.2	1.67	24.2	1.49	2008OCT20
16.864−2.159	18 29 24.42	-15 16 04.5	14.0	20.0	15.0	28.93	-	-	2008OCT20; (W98)
16.976−0.005	18 21 44.68	-14 09 48.5	5.0	9.0	6.5	0.64	6.6	0.70	2008OCT20
17.021−2.403	18 30 36.30	-15 14 28.5	17.0	25.0	23.6	4.90	-	-	2008OCT20
17.029−0.071	18 22 05.21	-14 08 51.0	90.4	96.0	91.4	1.10	91.4	1.69	2008AUG23
17.638+0.157	18 22 26.30	-13 30 12.1	20.0	22.0	20.8	24.79	20.8	34.17	C2009
17.862+0.074	18 23 10.10	-13 20 40.8	107.3	119.6	110.6	1.44	110.5	1.42	2008AUG23
18.073+0.077	18 23 33.98	-13 09 25.0	44.0	57.5	55.6	5.74	55.8	6.00	2008OCT20
18.159+0.094	18 23 40.18	-13 04 21.0	54.0	60.0	58.4	8.46	59.0	10.25	2008AUG23
18.262−0.244	18 25 05.70	-13 08 23.2	72.0	81.0	74.3	22.48	74.2	22.98	2008AUG23
18.341+1.768	18 17 58.13	-12 07 24.8	26.0	32.0	28.0	96.21	28.1	99.28	2008AUG23; (B02)
18.440+0.045	18 24 23.32	-12 50 52.1	57.0	66.0	61.8	1.85	61.8	2.45	2008AUG23
18.460−0.004	18 24 36.34	-12 51 08.6	46.7	50.0	49.4	24.23	49.4	25.30	2008AUG23; (W98)
18.661+0.034	18 24 51.10	-12 39 22.5	76.0	83.0	79.0	8.87	79.0	8.00	2008AUG23;
18.667+0.025	18 24 53.78	-12 39 20.4	76.1	81.0	76.6	8.71	76.6	8.78	2008AUG23
18.733−0.224	18 25 55.53	-12 42 48.9	44.0	49.0	45.8	2.34	45.9	2.30	2008AUG23;
18.735−0.227	18 25 56.46	-12 42 50.0	36.3	38.5	37.9	4.71	38.2	3.59	2008AUG23;
18.834−0.300	18 26 23.66	-12 39 38.0	37.5	44.0	41.3	5.01	41.2	7.47	2008AUG23
18.874+0.053	18 25 11.34	-12 27 36.8	37.7	40.6	38.7	12.77	38.7	9.80	2008AUG23
18.888−0.475	18 27 07.85	-12 41 35.9	53.0	57.6	56.5	5.70	56.4	5.56	2008AUG23
18.999−0.239	18 26 29.24	-12 29 07.1	65.0	69.8	69.4	1.05	69.4	0.90	2008AUG23
19.009−0.029	18 25 44.78	-12 22 46.1	53.0	63.0	55.4	19.32	55.4	20.39	2008AUG23
19.249+0.267	18 25 08.02	-12 01 42.2	12.5	21.0	19.9	2.32	19.8	3.35	2008AUG23
19.267+0.349	18 24 52.38	-11 58 28.2	12.5	17.5	16.2	5.33	16.3	3.40	2008AUG23
19.365−0.030	18 26 25.79	-12 03 52.0	24.0	30.0	25.3	33.83	25.3	34.16	2008AUG23; (W98)
19.472+0.170n	18 25 54.72	-11 52 33.0	17.0	23.0	21.7	17.97	21.7	15.06	C2009; (2008AUG23)
19.472+0.170	18 25 54.49	-11 52 36.5	12.7	17.7	13.8	3.30	13.8	1.97	C2009
19.486+0.151	18 26 00.39	-11 52 22.6	19.0	27.5	20.6	6.04	20.9	5.00	C2009
19.496+0.115	18 26 09.16	-11 52 51.7	120.0	122.0	121.2	7.55	121.3	5.60	C2009
19.609−0.234	18 27 37.99	-11 56 37.6	36.0	42.0	40.2	0.65	40.2	1.00	2007JUL21
19.612−0.120	18 27 13.48	-11 53 15.7	52.5	53.5	53.1	0.93	53.0	0.98	W98
19.612−0.134	18 27 16.52	-11 53 38.2	49.0	61.0	56.5	12.48	56.5	11.74	2007JUL21; (W98)
19.614+0.011	18 26 45.24	-11 49 31.4	30.8	34.8	32.8	3.99	32.9	3.80	2008AUG23
19.667+0.114	18 26 28.97	-11 43 48.9	13.4	17.8	14.2	2.20	16.3	1.52	2010MAY22
19.701−0.267	18 27 55.52	-11 52 40.3	41.5	46.5	43.9	10.72	43.8	11.72	2007JUL21; (W98)
19.755−0.128	18 27 31.66	-11 45 55.0	115.5	124.0	123.1	3.63	123.1	2.31	2008AUG23
19.884−0.534	18 29 14.37	-11 50 23.0	46.0	48.0	46.8	4.74	46.8	6.83	2008AUG23; (B02)

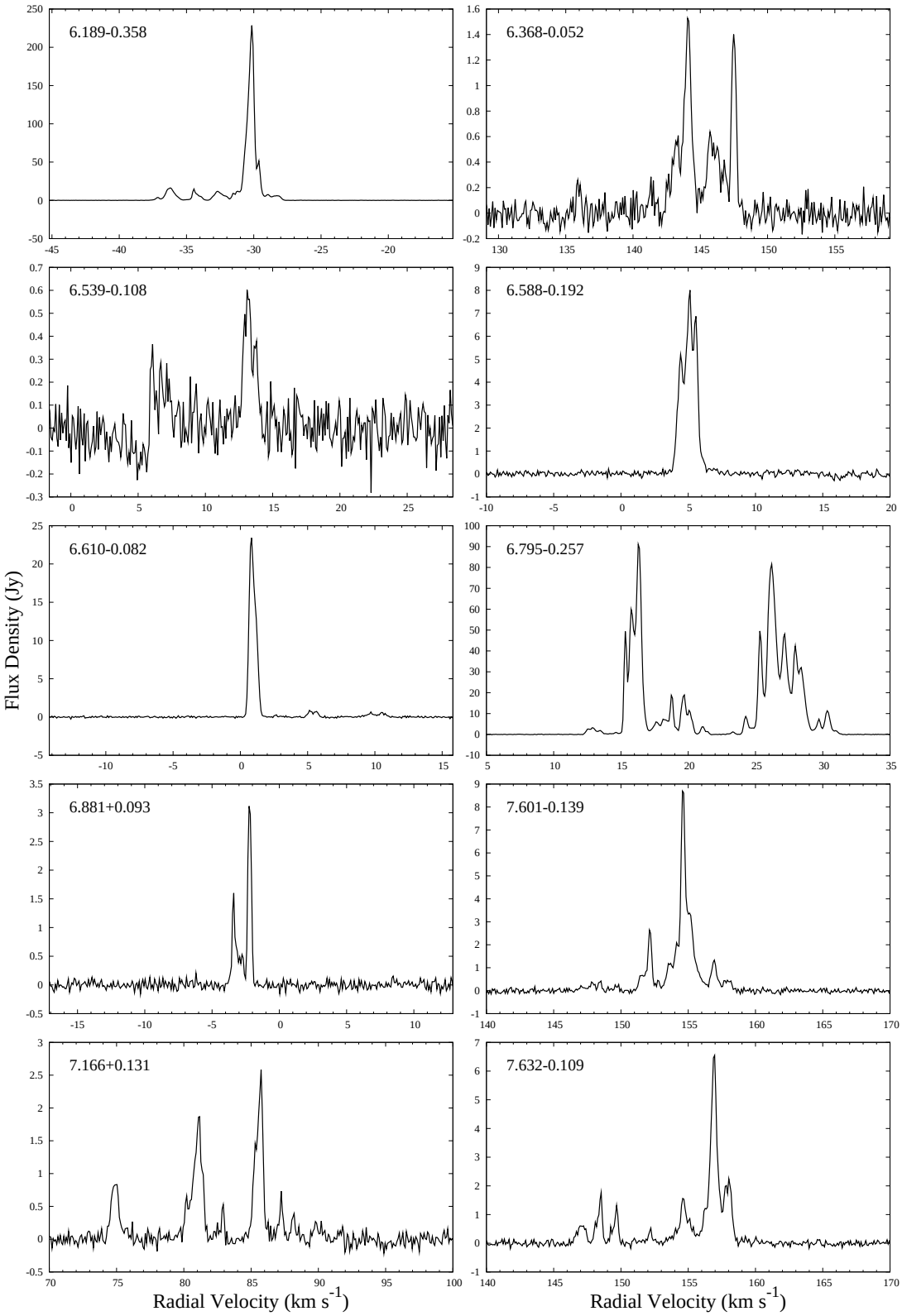

Figure 1. Spectra of 6668-MHz methanol masers. All spectra are from the MX observations unless stated otherwise.

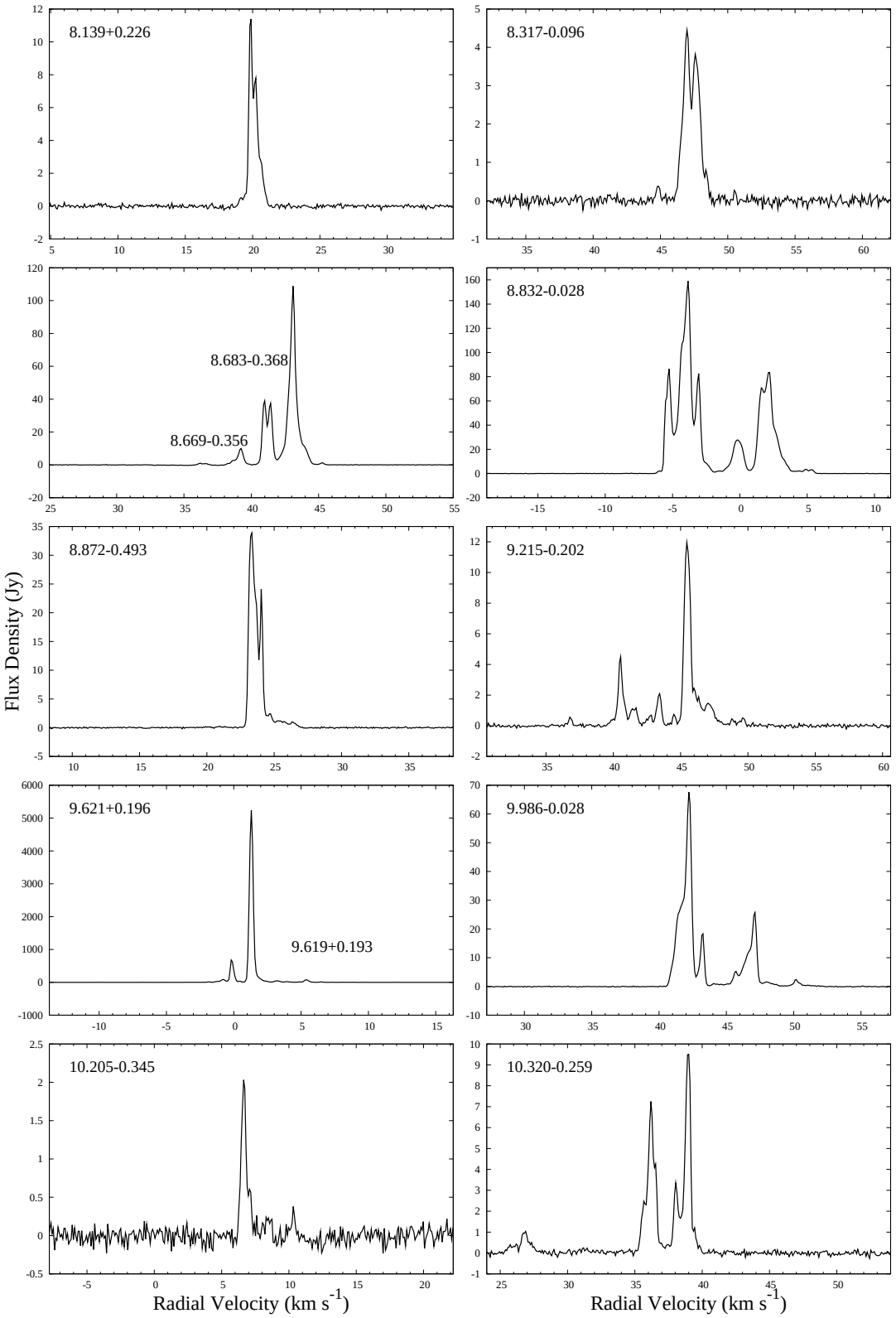

Figure 1. Spectra of 6668-MHz methanol masers.

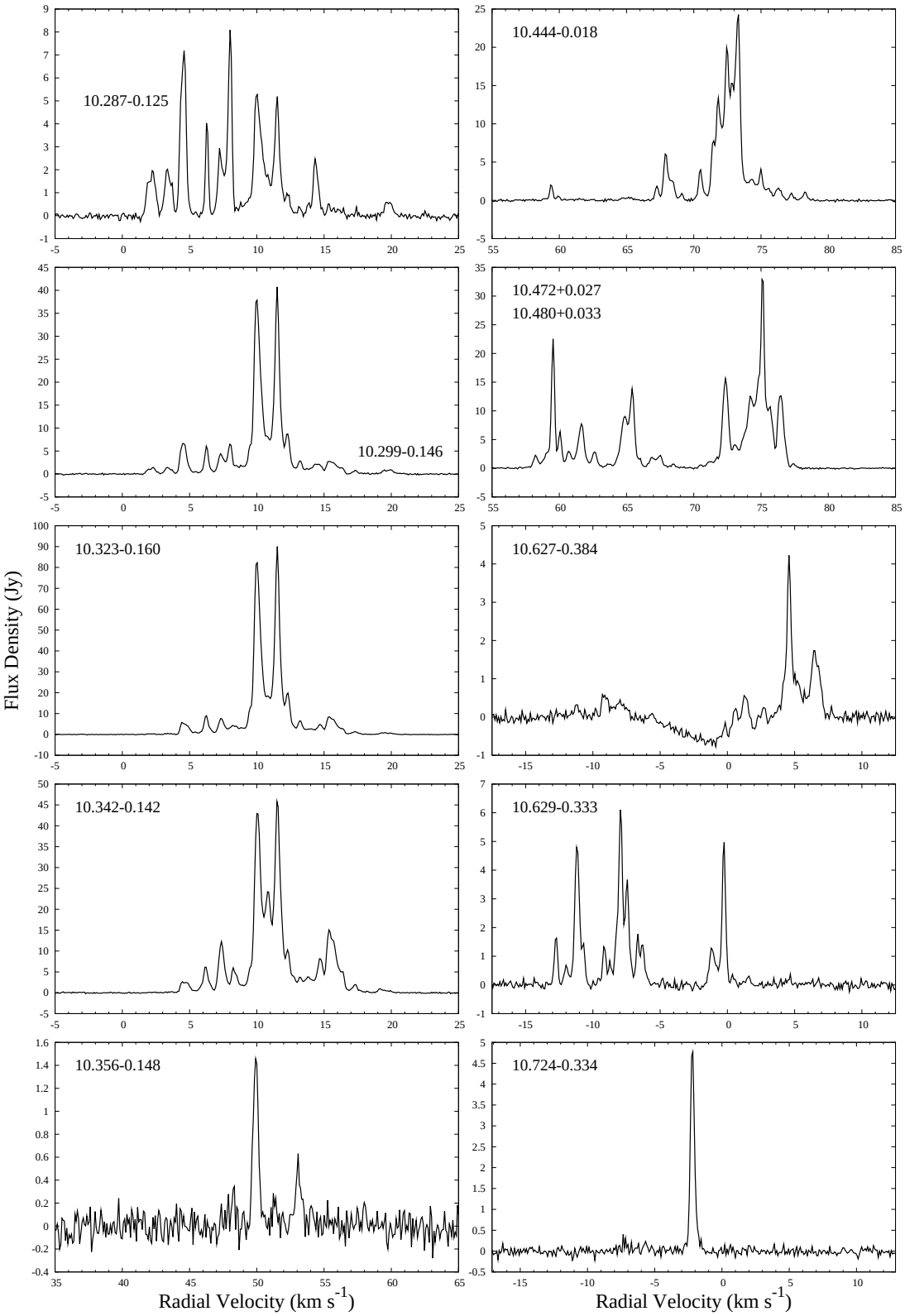

Figure 1. Spectra of 6668-MHz methanol masers.

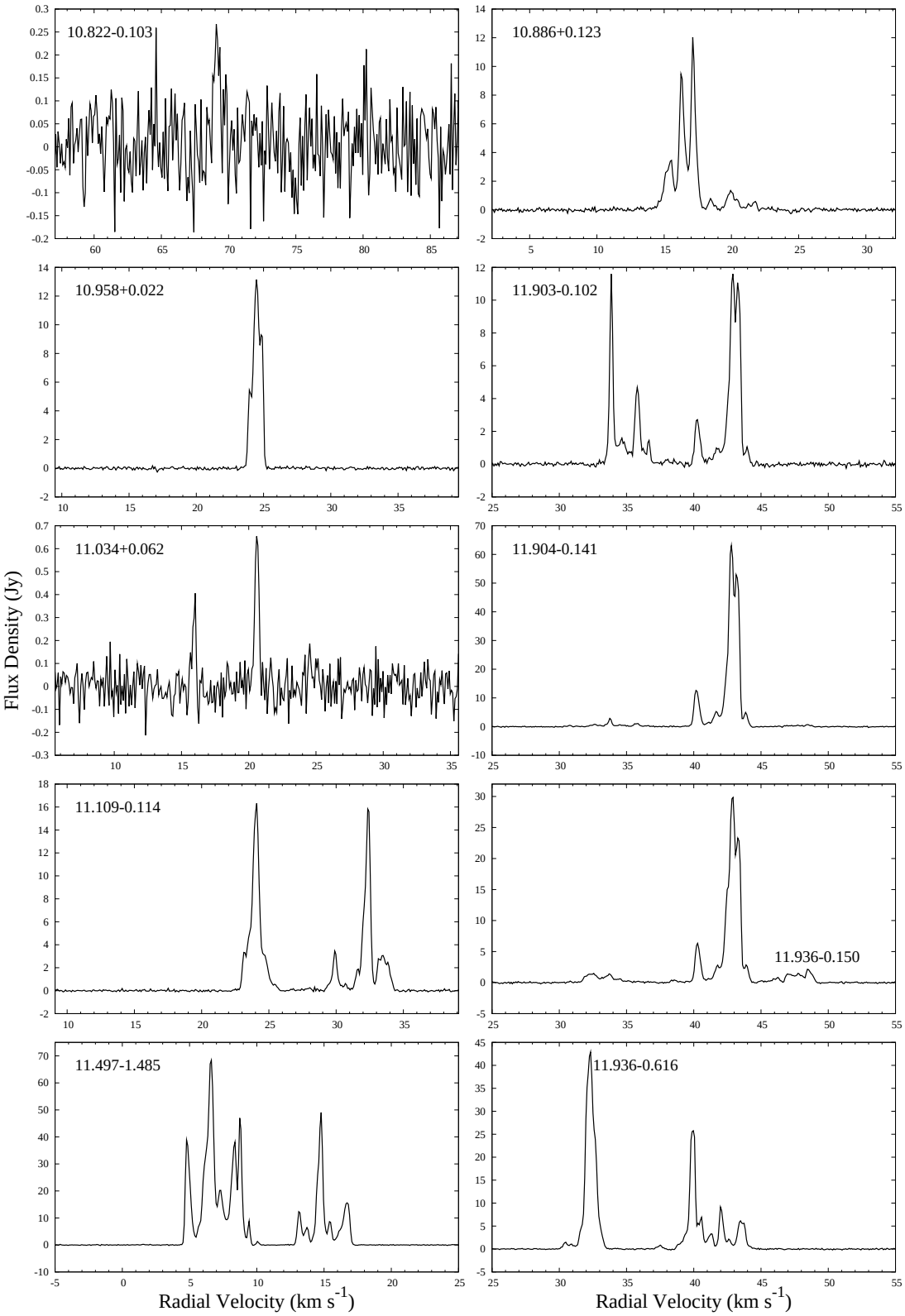

Figure 1. Spectra of 6668-MHz methanol masers.

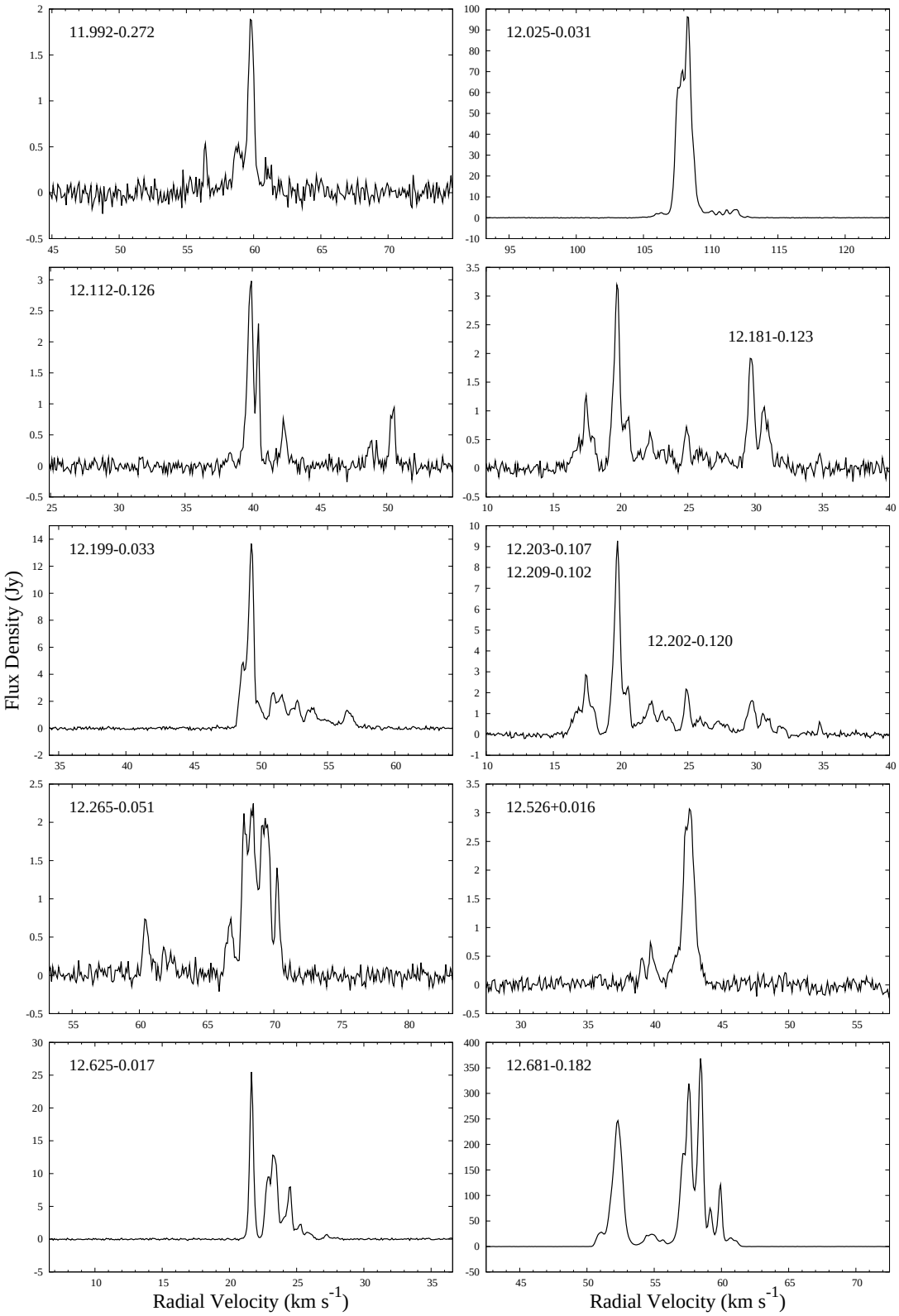

Figure 1. Spectra of 6668-MHz methanol masers.

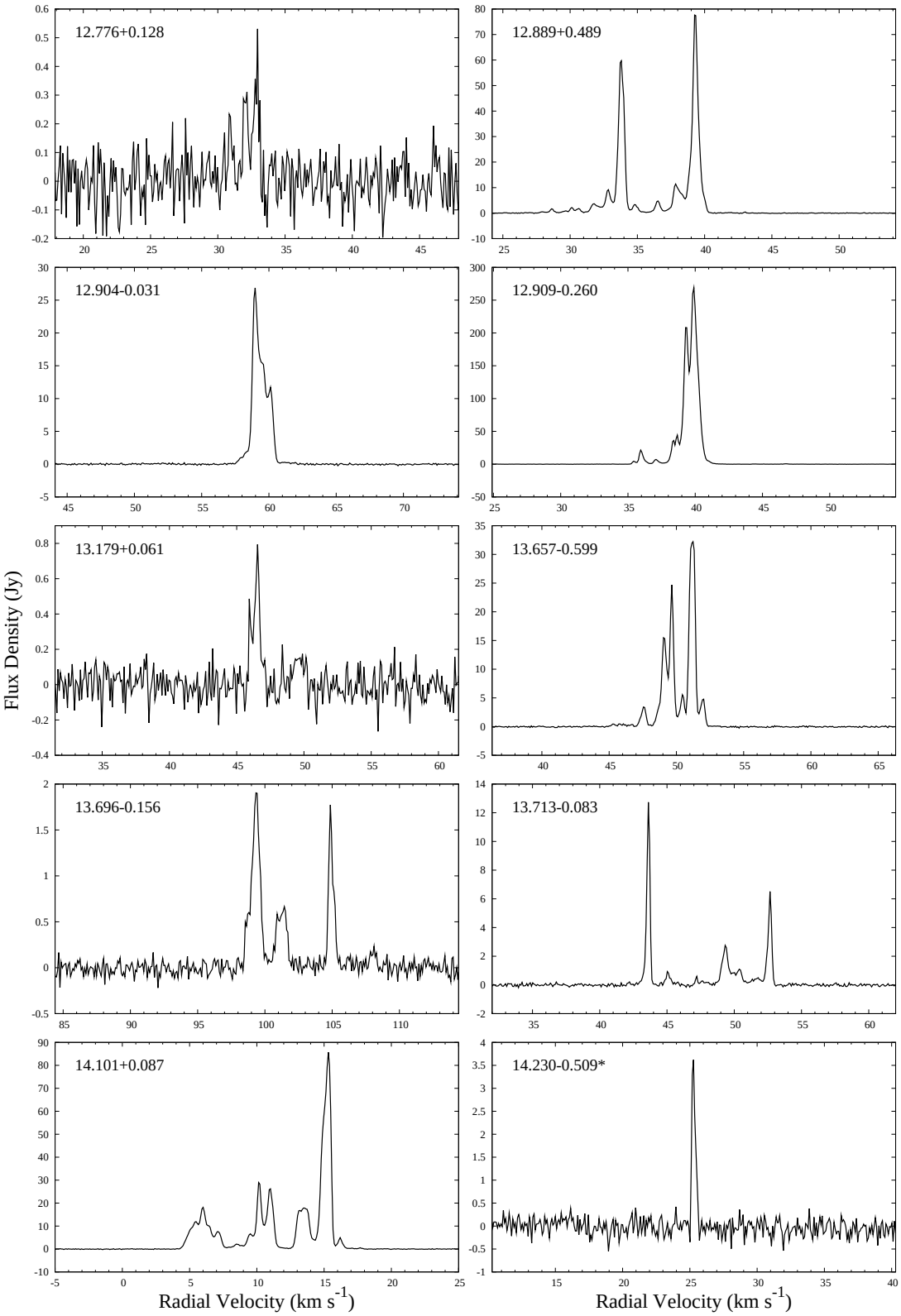

Figure 1. Spectra of 6668-MHz methanol masers. * denotes survey cube spectrum (source undetected in MX).

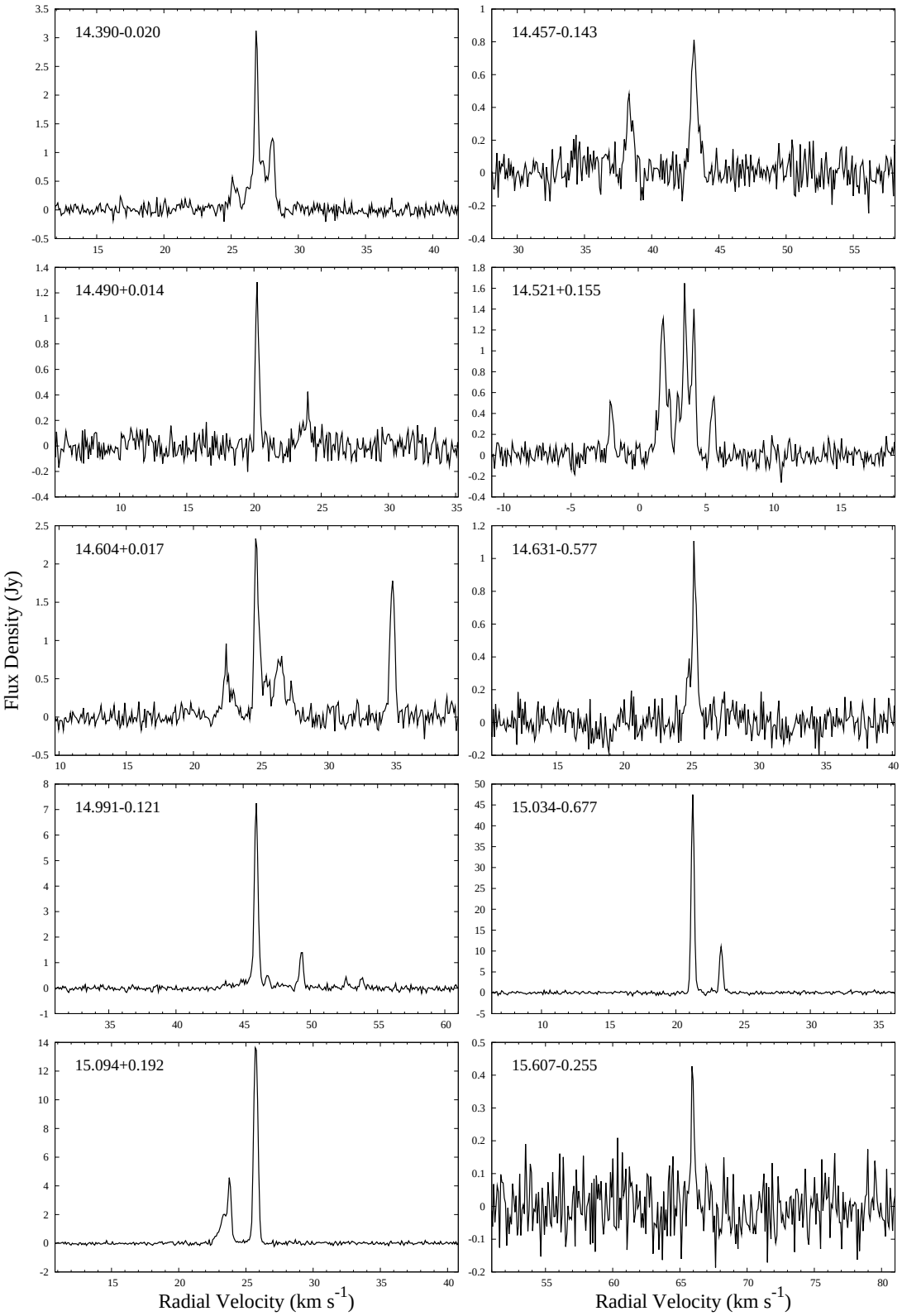

Figure 1. Spectra of 6668-MHz methanol masers.

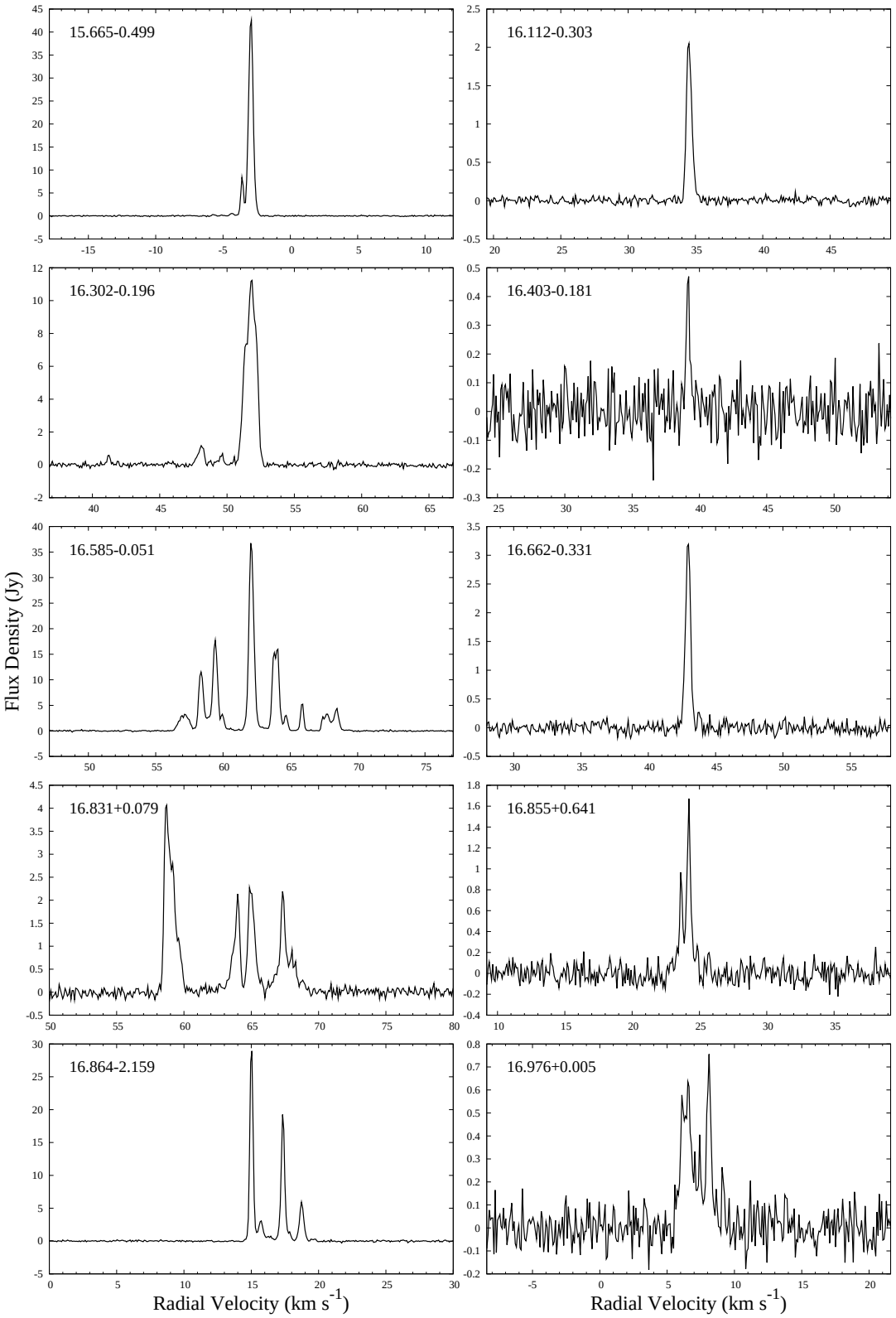

Figure 1. Spectra of 6668-MHz methanol masers.

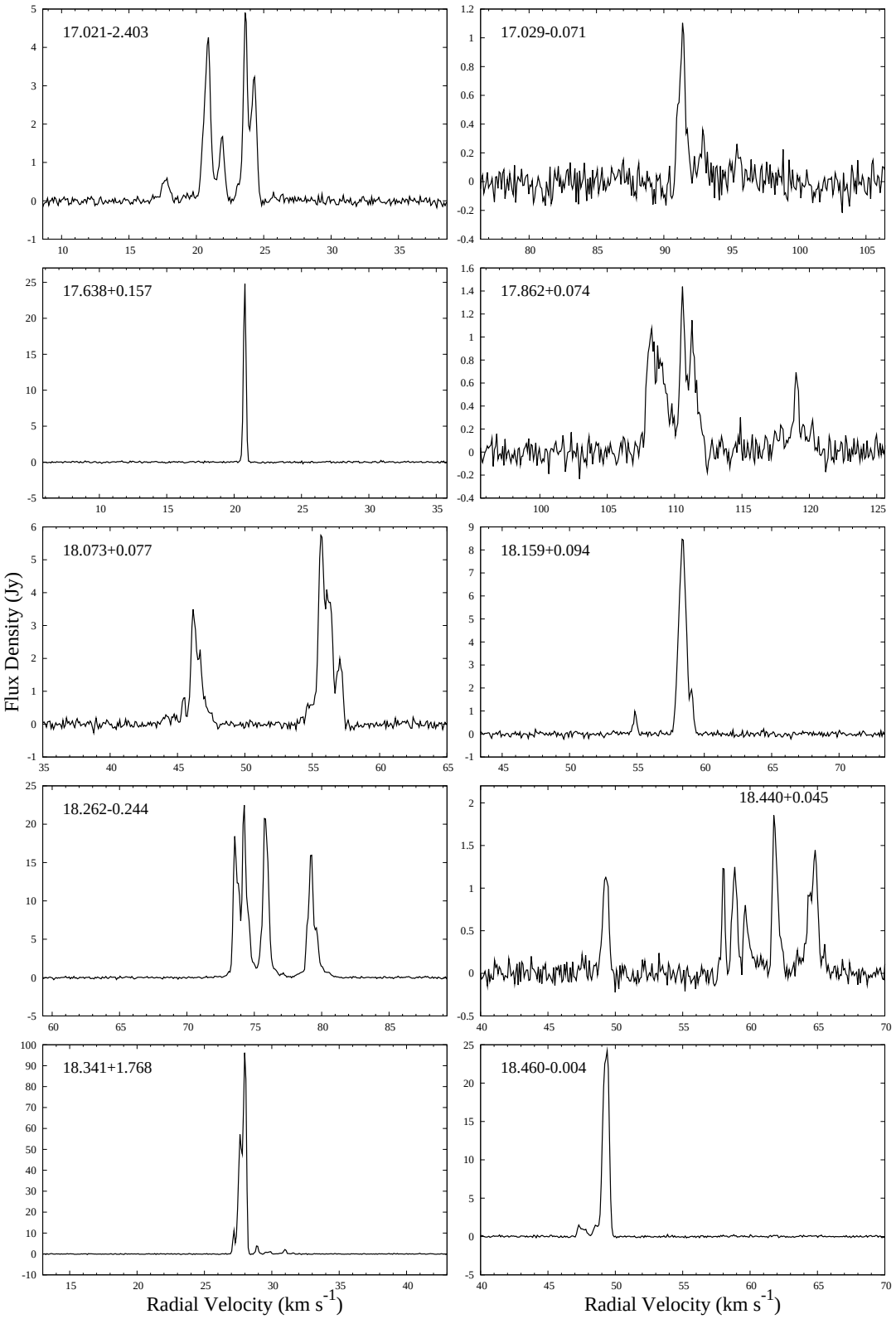

Figure 1. Spectra of 6668-MHz methanol masers.

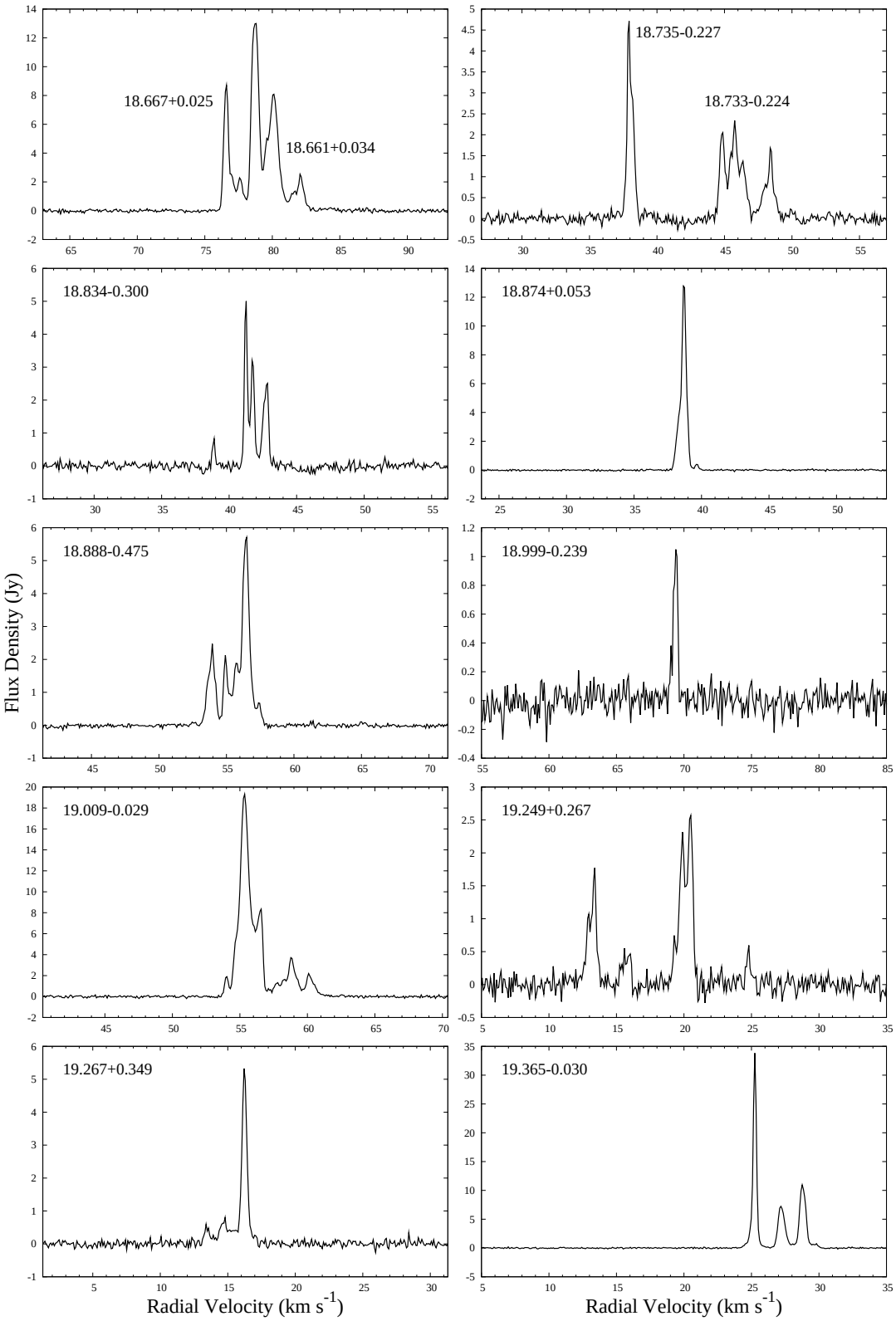

Figure 1. Spectra of 6668-MHz methanol masers.

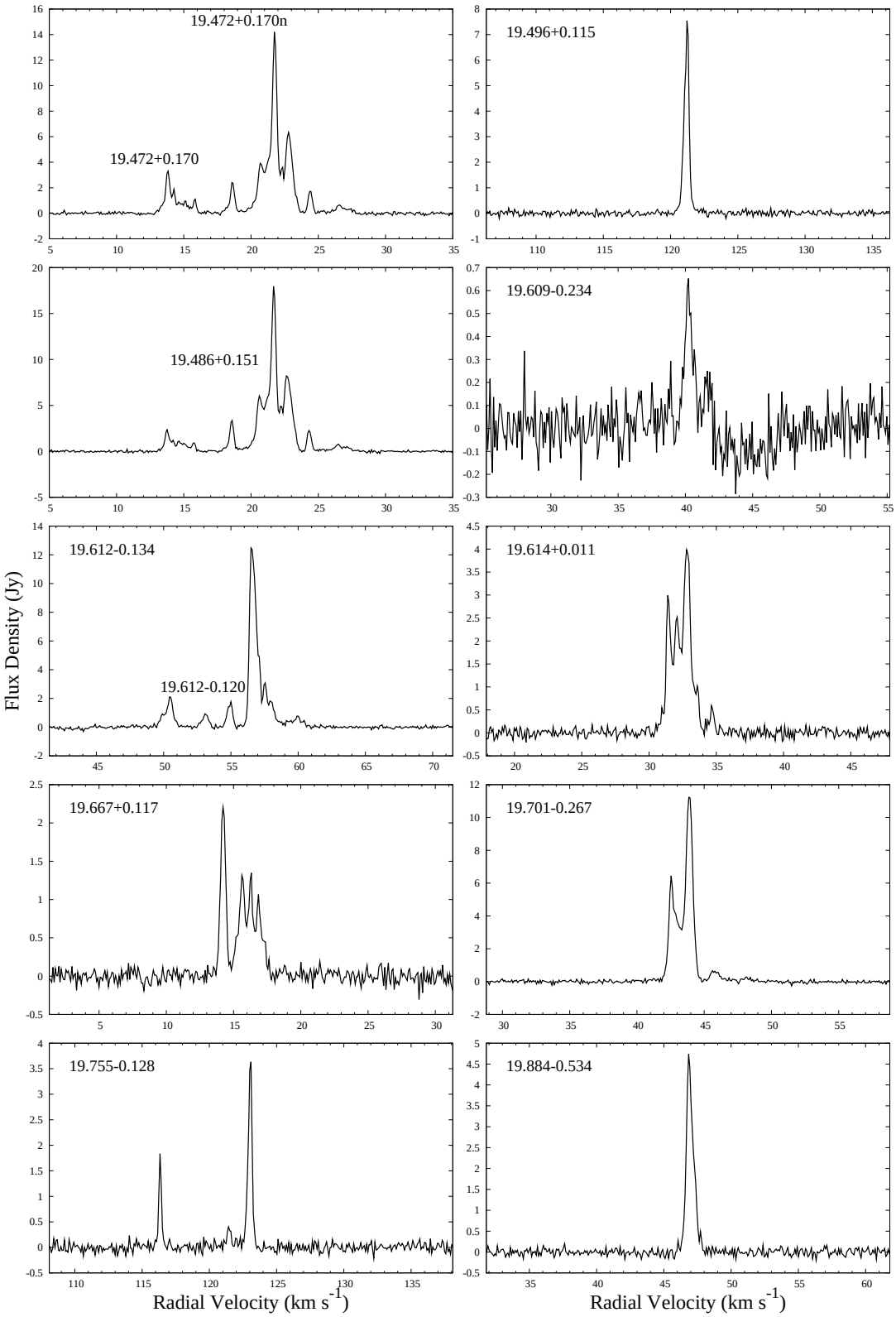

Figure 1. Spectra of 6668-MHz methanol masers.

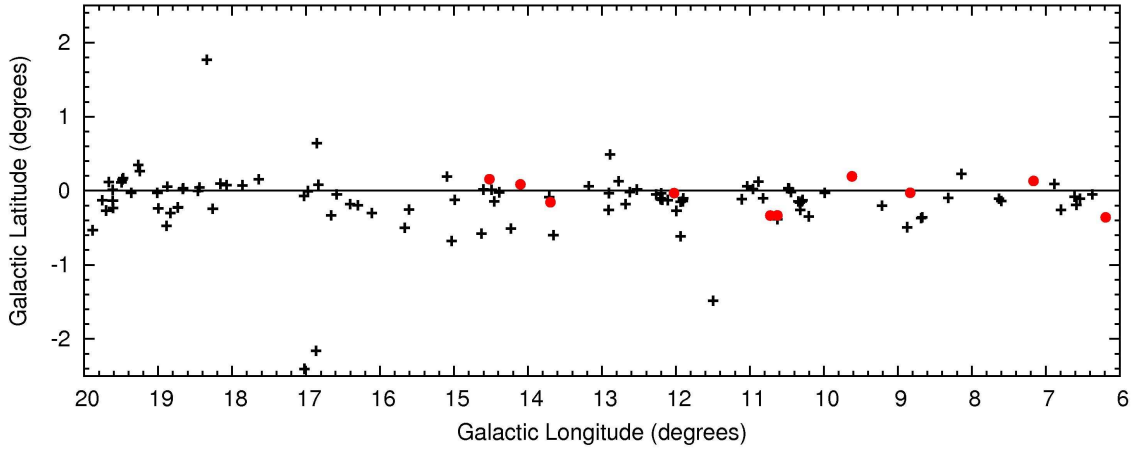

Figure 2. Longitude-latitude distribution of sources in the region 6° to 20°. Circles represent sources associated with the 3-kpc arms (Green et al. 2009b).

to have a survey cube peak flux density of ∼5200 Jy. The brightest new source detected in the survey is 6.189-0.358 with a survey cube peak flux density of ∼220 Jy (and an MX flux density of ∼230 Jy). The weakest known source in this region is 6.539-0.108 with a survey cube peak flux density of 0.5 Jy (and an MX flux density of 0.6 Jy). The weakest new detection in the region is 16.983+0.000 with a survey cube peak flux density of 0.7 Jy (0.64 Jy in the follow-up MX observation). Comparable to the 345° to 6° region we had only three new sources with peak flux densities above 20 Jy: 6.189-0.358, 8.832-0.028 and 8.872-0.493, with survey cube flux densities of 222 Jy, 127 Jy and 27 Jy respectively. There were four sources at or below the survey cube 4 sigma sensitivity limit of 0.7 Jy, two new (16.403-0.181 and 16.976-0.005) and two known (6.539-0.108 and 12.202-0.120). All four sources were confirmed with the higher sensitivity MX observations and ATCA positioning observations.

4.3 Variability

The ratio of peak flux density between the survey cube and the MX observations has a median value of 1.01. Only six sources varied by a factor of 2 or greater, two sources increasing, four decreasing (Fig. 3). The two that increased were: 8.139+0.226, which had an MX flux density twice that of the survey cube flux density; and 10.724-0.334, which had an MX peak flux density three times the survey cube value. The four sources which significantly decreased consisted of two with reduced emission and two which disappeared below the detection threshold of the survey. Both 10.822-0.103 and 12.904-0.031 decreased their emission by a factor of $\geqslant$2 (0.9 to 0.3 Jy and 40 to 20 Jy respectively). The two sources which dropped below our detection threshold represent ideal candidates for variability studies. The first was the new source 14.230-0.509, which had four epochs of observations: it was seen in the survey cube (2007 August) at 3.62 Jy (3 channels > 2 Jy) then subsequently not seen with the ATCA in 2008 October, before being seen again in 2009 January with the ATCA at 1.4 Jy and then not seen again in 2009 March in an MX observation with Parkes. The second was the new source 15.607-0.255, also with four epochs of observations: it was seen in the survey cube data (2007 August) at 0.85 Jy, then reduced to 0.43 Jy in the 2008 March MX before being undetectable in the 2008 August MX (i.e. <0.2 Jy) then rising again to ∼0.4 Jy in the ATCA observation in 2008 October.

In addition to those already mentioned, a further seven sources within longitudes 6° to 20° are known to be variable (and are individually noted in Section 3.1). Of special note 9.621+0.196 has been shown to periodically flare every 244 days (Goedhart et al. 2004; van der Walt et al. 2009), with possible coincident variability in the magnetic field (Vlemmings et al. 2009). Our survey cube observations were taken 2007 July 8, MJD 54289.5, lying within the rise of the flare (van der Walt et al. 2009) with the maser having a peak flux density of ∼5200 Jy. The MX observation was taken 2008 March 17, MJD 54542.5, lying within the rise of the subsequent flare, i.e. separated by approximately a full period from the original observation, again with a peak flux density of ∼5200 Jy. 12.889+0.489 has also been shown to have a periodic flare, with a period of 29.5 days (Goedhart et al. 2004, 2009). Our survey cube observation was made 2007 August 26, MJD 54338.5, measuring a peak flux density of 79 Jy for the 39.2 km s^{-1} feature. Assuming the 29.5 day period and the time series of Goedhart et al. (2009), our survey cube observation is likely to lie in the declining part of a flare. Our MX observation was made 2008 March 17, MJD 54917.5, measuring a peak flux density of 69 Jy for the same feature. According to the time series of Goedhart et al. (2009) this would place it on the rise of a flare.

4.4 Individual source velocity spreads

Figure 1 shows that the spectra of the masers comprise many narrow spectral features with individual widths often as small as ∼0.3 km s^{-1}, spread over a range of velocities. The total velocity spread in an individual source is dependent on the sensitivity of the observation and can also change as a result of intrinsic variability of the components (Section 4.3). Therefore, the velocity ranges listed in Table 1 are the widest velocity spread over which emission

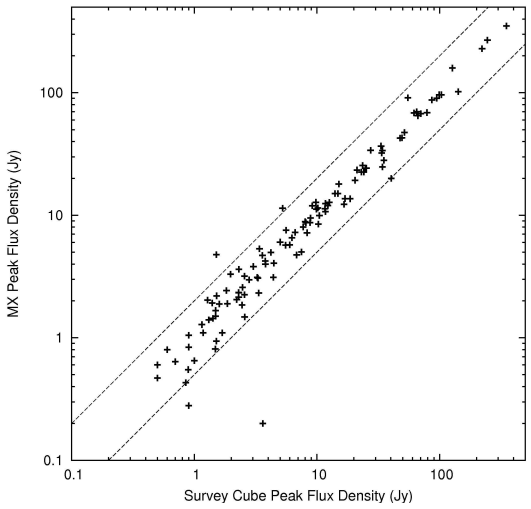

Figure 3. Variability in source peak flux density between the initial survey observations (Survey Cube) and the later targeted observations (MX) for 6° to 20° longitude. The dashed lines delimit a factor of 2 variability. The wider spread for weaker sources is likely due to the larger effect of noise variations on the survey cube spectra at these lower flux densities.

has been detected, considering all the observations available. This is the same convention as used for the masers in the Galactic centre (Caswell et al. 2010). The mean spread in velocity for a source is 7.2 km s^{-1}, the median is 6.0 km s^{-1}, and 70% of the sources have emission spread over velocity ranges less than 10 km s^{-1}. Only three sources of the 119 (<3%) have ranges greater than 16 km s^{-1}: 6.795-0.257 (19.3 km s^{-1}), 7.166+0.131 (16.5 km s^{-1}) and 10.472+0.027 (20.1 km s^{-1}). This rarity in velocity spreads greater than 16 km s^{-1} is comparable to both Caswell (2009) (<3%) and Caswell et al. (2010) (∼1%).

4.5 Distribution of velocities

Consistent with the results for the central part of the Galaxy (Caswell et al. 2010), all the masers in the longitude range 6° to 20° lie well inside the velocity coverage of the MMB (which was chosen to fully sample the velocity range of the CO emission of Dame et al. 2001). There are three sources in the region with velocities of peak emission exceeding 125 km s^{-1} (6.368-0.052, 7.601-0.139 and 7.632-0.109) and there are six sources with negative velocities of peak emission (6.189-0.358, 6.881+0.093, 8.832-0.028, 10.629-0.333, 10.724-0.334 and 15.665-0.499). Only one of the six sources has a significantly negative velocity (<-10 km s^{-1}), 6.189-0.358.

4.6 Tracing Galactic structure

6668-MHz methanol masers have the potential to trace the kinematics of Galactic structure: their velocities are closely linked to the systemic velocities (Szymczak et al. 2007; Pandian et al. 2009); and they are only detected towards regions of high-mass star formation (Pestalozzi et al. 2002; Minier et al. 2003; Xu et al. 2008), regions which are intrinsically associated with the spiral arms. Figure 4 shows longitudes and velocities of the 6668-MHz methanol sources detected with the MMB survey between longitudes 345° and 20° (this paper and Caswell et al. 2010). The masers are shown in relation to the 3-kpc arms as defined by Dame & Thaddeus (2008) and the spiral arm loci based on the logarithmic spirals of Georgelin & Georgelin (1976), with the updates of Taylor & Cordes (1993) and the rotation curve of Brand & Blitz (1993) with IAU standard LSR parameters. Figure 4 includes an inset of the assumed spiral arm pattern, oriented so as to readily recognise how individual portions of the arms transform to the *l,v* domain. By plotting in the *l,v* domain we can investigate Galactic structure without the need to correctly assign individual sources to near and far kinematic distances. The figure shows that there appear to be masers lying between the arms, but before closer inspection of individual anomalies, there are two issues that one must be aware of: the thickness of the arm loci and the choice of rotation curve. Firstly, the arms plotted in *l,v* diagrams are purposely thin to reduce obscuration, but as such they do not account for the real spatial radial thickness and velocity dispersion within the arms. Secondly, the locations (physical and in the *l,v* domain) of the arms depends on the Galactic rotation curve adopted. If the spiral pattern is broadly correct, any change in adopted rotation curve will only alter the position of the arms slightly, leaving them as continuous structures, not only in the Galactic disk, but also in the *l,v* domain. For the Galactic structure investigation presented here we use the Brand & Blitz (1993) curve, since it closely approximates the assumptions made in deriving the spatial pattern of the spiral arms. Furthermore we resist adopting the most recently suggested rotation curve and revised LSR suggested by Reid et al. (2009), as it is preliminary and requires revision (McMillan & Binney 2010). However, we note that near the Galactic Centre, where we did choose the Reid et al. parameters (Caswell et al. 2010), this choice had negligible impact on the interpretation of that region. It would affect the current discussion in only one instance (noted below), but would have more impact at longitudes further from the Galactic centre.

4.6.1 The 3-kpc arm (expanding ring)

Table 2 lists 45 sources associated kinematically and spatially with the 3-kpc arm features (denoted by filled circles in Figure 4). This includes the 42 originally identified in Green et al. (2009b) and three additional sources, from Caswell et al. (2010) and the current paper. A further three sources (two new to the survey) between longitudes 15° and 20° (17.862+0.074, 19.496+0.115 and 19.755-0.128) have velocities in excess of 100 km s^{-1} and are potential candidates of an extended 3-kpc structure. They do not align with spiral arm loci (subject to the caveats already mentioned), but they could be accounted for by the far side of the 3-kpc arms if this is extended as a continuous ring structure with a radius of ∼3.5 kpc (e.g. Sevenster et al. 1999). An alternative explanation requiring a shift in velocity of the Crux-Scutum arm (by ∼30 km s^{-1}) seems less likely. Also within the 15° and 20° longitude range are eight sources with velocities between 60 km s^{-1} and 100 km s^{-1} (15.607-0.255, 16.585-0.051,16.831+0.079, 17.029-0.071, 18.262-0.244, 18.661+0.034,18.667+0.025 and

18.999-0.239) and seven sources with velocities between $35\,\mathrm{km\,s^{-1}}$ and $50\,\mathrm{km\,s^{-1}}$ (16.112-0.303, 18.735-0.227, 18.834-0.300, 18.874+0.053, 19.609-0.234, 19.614+0.011 and 19.701-0.267) which do not align with spiral arm loci. These sources may also be accounted for by the continuation beyond 15° of the 3-kpc arms structure as a ring. We note that if an alternative rotation model were adopted, the shift of the spiral arm loci might account for some of these sources, but would leave a different group of orphans. For example, using the IAU solar parameter values and flat rotation curve of Reid et al. (2009) would shift the loci of the Crux-Scutum and Carina-Sagittarius arms by about $+15\,\mathrm{km\,s^{-1}}$. This allows 16.585-0.051 ($62.1\,\mathrm{km\,s^{-1}}$), 16.831+0.079 ($58.7\,\mathrm{km\,s^{-1}}$), 18.999-0.239 ($69.4\,\mathrm{km\,s^{-1}}$) and 19.614+0.011 ($32.8\,\mathrm{km\,s^{-1}}$) to be associated with the arms, but disassociates 16.403-0.181 (peak velocity of $39\,\mathrm{km\,s^{-1}}$), 16.662-0.331 (peak velocity of $43\,\mathrm{km\,s^{-1}}$), 18.733-0.224 (peak velocity of $46\,\mathrm{km\,s^{-1}}$) and 19.884-0.534 (peak velocity of $47\,\mathrm{km\,s^{-1}}$). Hence, regardless of parameter and model choice, there are 18 sources unaccounted for by the spiral arms which are candidates for an extended 3-kpc arm structure.

The actual structure of the 3-kpc arms has been variously interpreted as an expanding ring (requiring an explosive precursor), as material orbiting a bar (either on a circular orbit or an elliptical orbit with its major axis parallel to the bar) and as (lateral) arms flowing from the ends of the bar. These physical interpretations attempt to explain the structure seen in longitude-velocity space, most prominently the significant offset from $0\,\mathrm{km\,s^{-1}}$ at longitude 0°. This anomalous velocity either requires a circular orbit with a radial expansion of $\sim 50\,\mathrm{km\,s^{-1}}$ or an elliptical orbit with appropriate semi-major and minor axes and angle of inclination. Overall, the results from the MMB so far are in accord with the initial notion of the 3-kpc arms as simply an approximately circular ring uniformly expanding (van der Kruit 1971). More elegant physical descriptions, such as elliptical orbits, appear to have difficulty accounting for the observations. As an example, we cite a recent suggestion by Rodriguez-Fernandez & Combes (2008). The l-v plot corresponding to their orbits is shown in grey in Figure 4. This model is based on a gas flow model of the 2MASS star count with a disk, bulge and nuclear bar and comprises arms which extend around the bar forming an ellipse. In this particular example the negative longitudes of the near arm and the positive longitudes of the far arm match both the CO emission (light blue shading in Figure 4) and the 3-kpc maser distribution well. However, for the far arm at negative longitudes the model deviates significantly from the CO emission (although in doing so it does align with a number of masers at approximately −10° and velocities between $-50\,\mathrm{km\,s^{-1}}$ and $-100\,\mathrm{km\,s^{-1}}$). Similarly, for the near arm at positive longitudes, the model also deviates significantly from the CO (although it is possible that modifying the bar characteristics within the model may account for the higher maser density seen between longitudes 10° and 15°). We are currently incorporating MMB data from beyond the longitude range 345° to 20° into a more comprehensive analysis of the 3-kpc arms, which will be described fully in a later publication.

4.6.2 The Galactic Bar

Figure 4 highlights seven sources with velocities greater than those of the far 3-kpc arm. Four are previously known and have been associated with the Galactic bar (see Caswell et al. 2010 for details). The other three are newly detected sources between longitudes 6° and 7°. These three sources (6.368-0.052, 7.601-0.139, 7.632-0.109) are also likely to be associated with the bar, having kinematics which fit the near-side of orbits following a barred potential (e.g. Binney et al. 1991; Fux 1999). The bar is now traced by methanol masers over the longitude range −5.3° to +7.6°. Emission from an HII region provides evidence that star formation in the bar can also be traced at large negative velocities exceeding $-200\,\mathrm{km\,s^{-1}}$ (Caswell & Haynes 1982). However, we do not detect any maser emission near these velocities.

Two of the bar sources (354.701+0.299 and 354.724+0.300) are spatially and kinematically associated with the high velocity CO emission feature identified by Bania (1977) and labelled as 'Clump 1'. The compression and perturbation of Clump 1 would suggest star formation (Fux 1999, and references therein) and the presence of 6.7-GHz methanol maser emission confirms it. We do not detect any masers coincident with the second of Bania's CO structures, 'Clump 2'. The high range of velocities ($>100\,\mathrm{km\,s^{-1}}$) and small spatial extent of this clump, could be indicative of conditions too turbulent for the coherence necessary for maser emission.

4.6.3 Orientation of the Bar

The most densely populated portion of the far 3-kpc arm is between longitudes -10° and -15°. This may correspond to enhanced high-mass star formation at the end of the Galactic bar, where the bar meets the 3-kpc arms (Caswell et al. 2010). This interpretation depends on the inclination of the Galactic bar to the Sun-Galactic centre line-of-sight as well as its length. Both of these are still a matter of debate, with the orientation varying between 15° and 45° (e.g. Peters 1975; Binney et al. 1991; Fux 1999; Englmaier & Gerhard 1999; Rodriguez-Fernandez & Combes 2008), and the half-length between 2 and 5 kpc. However, the bar descriptions fall into two main categories: a short, bulge-like bar with an orientation of 20°-25° (e.g. Bissantz & Gerhard 2002; Babusiaux & Gilmore 2005) and/or a long, thin bar with an orientation of ∼45° (e.g. Hammersley et al. 2000; Benjamin et al. 2005).

A bar orientation within the range 20°-25° (and a half-length of 2.5 kpc) would imply the near-side bar end lying between 8° and 10° longitude and the far-side bar end lying between -4.5° and -6° longitude. We find no corresponding high density regions: there are only three masers associated with the near-side and one with the far-side. A bar orientation of approximately 45° (and a half-length of 3.5 kpc) would imply a near-side bar end at 22° longitude and a far-side bar end at -12° longitude. The extent of velocities for the near-side would depend on the nature of the 3-kpc arm structure beyond 15°, but we do find a high density of masers at longitudes 18° to 20° with velocities between $10\,\mathrm{km\,s^{-1}}$ and $60\,\mathrm{km\,s^{-1}}$ (20 masers). The far-side is

Table 2. Sources associated with the 3-kpc arms as identified by Green et al. (2009b) and Caswell et al. (2010). For source details see: [1]this paper; [2]Caswell et al. (2010).

Name (l, b)	V_{pk} ($km\,s^{-1}$)	V_{mid} ($km\,s^{-1}$)	S_{pk} (Jy)	Arm
000.212−0.001[2]	49.5	45.8	2.40	Far
002.143+0.009[2]	62.7	59.5	6.70	Far
003.442−0.348[2]	-35.2	-35.0	0.66	Near
005.618−0.082[2]	-27.1	-23.3	3.42	Near
006.189−0.358[1]	-30.2	-32.3	221.60	Near
007.166+0.131[1]	85.7	83.1	2.47	Far
008.832−0.028[1]	-3.8	-1.6	126.80	Near
009.619+0.193[1]	7.0	5.5	5.5	Near
009.621+0.196[1]	1.3	2.1	5196.00	Near
010.629−0.333[1]	-0.4	-6.4	4.20	Near
010.724−0.334[1]	-2.1	-2.1	1.51	Near
012.025−0.025[1]	108.3	109.2	103.10	Far
013.696−0.156[1]	99.4	102.0	1.86	Far
014.101+0.087[1]	15.4	10.5	86.55	Near
014.521+0.155[1]	4.1	3.7	1.31	Near
345.198−0.030[2]	-0.5	-1.5	2.23	Far
345.441+0.205[2]	0.9	-5.5	2.32	Far
345.505+0.348[2]	-17.8	-16.8	307.00	Far
345.576−0.225[2]	-126.8	-124.6	0.65	Near
345.807−0.044[2]	-2.0	-1.8	1.21	Far
345.824+0.044[2]	-10.3	-10.5	3.92	Far
346.036+0.048[2]	-6.4	-9.2	10.42	Far
346.481+0.132[2]	-5.5	-8.3	1.48	Far
346.517+0.117[2]	-1.7	-1.0	4.00	Far
346.522+0.085[2]	5.7	5.4	1.47	Far
347.583+0.213[2]	-102.3	-99.9	3.18	Near
347.628+0.149[2]	-96.5	-96.9	18.98	Near
348.027+0.106[2]	-121.2	-118.6	4.54	Near
348.654+0.244[2]	16.9	17.0	0.99	Far
348.723−0.078[2]	11.5	10.5	2.25	Far
348.892−0.180[2]	1.5	1.5	2.44	Far
349.067−0.017[2]	11.6	11.0	2.43	Far
349.151+0.021[2]	14.6	19.6	3.33	Far
349.884+0.231[2]	16.2	15.5	6.42	Far
350.116+0.220[2]	4.2	4.0	2.31	Far
350.776+0.138[2]	38.7	36.8	0.91	Far
351.581−0.353[2]	-94.2	-94.5	47.46	Near
352.584−0.185[2]	-85.7	-86.2	3.73	Near
352.604−0.225[2]	-81.7	-83.0	1.80	Near
353.363−0.166[2]	-79.0	-79.2	2.94	Near
354.496+0.083[2]	27.0	22.5	7.78	Far
356.662−0.263[2]	-53.8	-50.5	10.10	Near
358.809−0.085[2]	-56.2	-55.4	11.99	Near
359.436−0.104[2]	-47.8	-49.0	59.70	Near
359.436−0.102[2]	-53.4	-56.0	1.50	Near

approximately coincident with the high density noted by Caswell et al. (2010).

4.7 Data Availability

The data from the MMB survey is being made publicly available as each section of the survey is published. The data are accessible from http://www.jb.man.ac.uk/mmb or http://www.astromasers.org.

5 SUMMARY

We present the 119 sources detected by the Methanol Multibeam survey between longitudes 6° and 20°, including 42 new detections. Consistent with expectations we find a narrow latitude distribution. We list the 45 sources within ±15° of the Galactic centre associated with the 3-kpc arm features. We associate sources with the Galactic bar and relate the higher density regions of the 3-kpc arms to the interaction of a Galactic bar at an orientation of ∼45°.

ACKNOWLEDGMENTS

AA acknowledges the support of a Science and Technology Facilities Council (STFC) studentship. LQ acknowledges the support of the EU Framework 6 Marie Curie Early Stage Training programme under contract number MEST-CT-2005-19669 "ESTRELA". The Parkes Observatory and the Australia Telescope Compact Array are part of the Australia Telescope which is funded by the Commonwealth of Australia for operation as a National Facility managed by CSIRO.

REFERENCES

Anderson L. D., Bania T. M., 2009, ApJ, 690, 706
Babusiaux C., Gilmore G., 2005, MNRAS, 358, 1309
Bania T. M., 1977, ApJ, 216, 381
Bania T. M., 1980, ApJ, 242, 95
Benjamin R. A., Churchwell E., Babler B. L., et al. 2005, ApJ Letters, 630, 149
Beuther H., Walsh A., Schilke P., Sridharan T. K., Menten K. M., Wyrowski F., 2002, A&A, 390, 289
Binney J., Gerhard O. E., Stark A. A., Bally J., Uchida K. I., 1991, MNRAS, 252, 210
Bissantz N., Gerhard O., 2002, MNRAS, 330, 591
Brand J., Blitz L., 1993, A&A, 275, 67
Caswell J. L., 1997, MNRAS, 289, 203
Caswell J. L., 2009, Publications of the Astronomical Society of Australia, 26, 454
Caswell J. L., Fuller G. A., Green J. A., et al. 2010, MNRAS, 404, 1029
Caswell J. L., Haynes R. F., 1982, ApJ Letters, 254, 31
Caswell J. L., Vaile R. A., Ellingsen S. P., Whiteoak J. B., Norris R. P., 1995a, MNRAS, 272, 96
Caswell J. L., Vaile R. A., Ellingsen S. P., 1995b, Publications of the Astronomical Society of Australia, 12, 37
Cohen R. J., Davies R. D., 1976, MNRAS, 175, 1
Cyganowski C. J., Brogan C. L., Hunter T. R., Churchwell E., 2009, ApJ, 702, 1615
Dame T. M., Hartmann D., Thaddeus P., 2001, ApJ, 547, 792
Dame T. M., Thaddeus P., 2008, ApJ Letters, 683, 143
Downes D., Wilson T. L., Bieging J., Wink J., 1980, A&As, 40, 379
Ellingsen S. P., 2007, MNRAS, 377, 571
Englmaier P., Gerhard O., 1999, MNRAS, 304, 512
Fish V. L., Reid M. J., Wilner D. J., Churchwell E., 2003, ApJ, 587, 701
Fux R., 1999, A&A, 345, 787
Georgelin Y. M., Georgelin Y. P., 1976, A&A, 49, 57

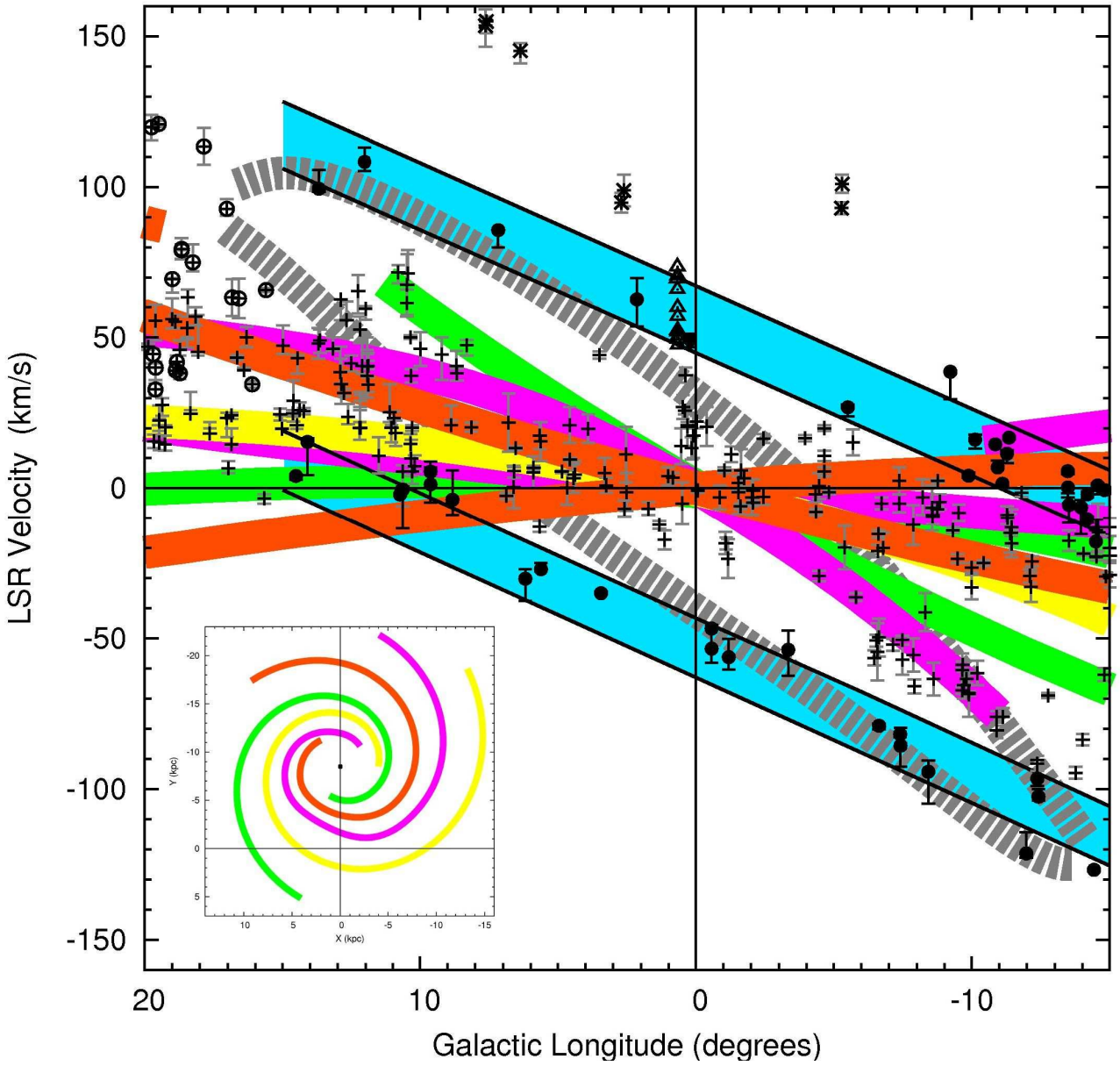

Figure 4. Longitude-Velocity 'crayon' plot showing Methanol Multibeam sources from the current paper and from Caswell et al. (2010). The coloured loci are the spiral arms (Yellow - Perseus; Purple - Carina-Sagittarius; Orange - Crux-Scutum; Green - Norma). The blue shading is the region identified in CO emission as the 3-kpc arms in Dame & Thaddeus (2008). Shown in broken grey is the locus of an elliptical interpretation of the 3-kpc arm structure (Rodriguez-Fernandez & Combes 2008). Masers are represented by crosses, with the exception of those associated with the 3-kpc arms (filled circles), Sagittarius B2 (open triangles) and the Galactic bar (stars). Crosses surrounded by open circles represent the unassociated sources discussed in Section 4.6.1. Grey error bars show the spread over velocity for maser emission. Inlay shows location of arms with respect to the sun (0,0), oriented with positive longitudes to the left in line with the l,v plot.

Goedhart S., Gaylard M. J., van der Walt D. J., 2003, MNRAS, 339, L33

Goedhart S., Gaylard M. J., van der Walt D. J., 2004, MNRAS, 355, 553

Goedhart S., Langa M. C., Gaylard M. J., van der Walt D. J., 2009, MNRAS, 398, 995

Green J. A., Caswell J. L., Fuller G. A., et al., 2009a, MNRAS, 392, 783

Green J. A., McClure-Griffiths N. M., Caswell J. L., Ellingsen S. P., Fuller G. A., Quinn L., Voronkov M. A., 2009b, ApJ Letters, 696, 156

Hammersley P. L., Garzón F., Mahoney T. J., López-Corredoira M., Torres M. A. P., 2000, MNRAS, 317, L45

Hofner P., Kurtz S., Churchwell E., Walmsley C. M., Cesaroni R., 1994, ApJ Letters, 429, 85

Kolpak M. A., Jackson J. M., Bania T. M., Clemens D. P., Dickey J. M., 2003, ApJ, 582, 756

van der Kruit P. C., 1971, A&A, 13, 405

Lockman, F.J., 1980, ApJ, 241, 200
MacLeod G. C., Gaylard M. J., 1992, MNRAS, 256, 519
McClure-Griffiths N. M., Dickey J. M., Gaensler B. M., Green A. J., Haverkorn M., Strasser S., 2005, ApJs, 158, 178
McMillan P. J., Binney J. J., 2010, MNRAS, 402, 934
Menten K. M., 1991, ApJ, 380, 75
Minier V., Ellingsen S. P., Norris R. P., Booth R. S., 2003, A&A, 403, 1095
Norris R. P., Whiteoak J. B., Caswell J. L., Wieringa M. H., Gough R. G., 1993, ApJ, 412, 222
Oort J. H., Kerr F. J., Westerhout G., 1958, MNRAS, 118, 379
Pandian J. D., Menten K. M., Goldsmith P. F., 2009, ArXiv e-prints
Pestalozzi M., Humphreys E. M. L., Booth R. S., 2002, A&A, 384, 15
Pestalozzi M. R., Minier V., Booth R. S., 2005, A&A, 432, 737
Peters III W. L., 1975, ApJ, 195, 617
Phillips C. J., Norris R. P., Ellingsen S. P., McCulloch P. M., 1998, MNRAS, 300, 1131
Reid M. J., Menten K. M., Zheng X. W., Brunthaler A., Moscadelli L., Xu Y., Zhang B., Sato M., Honma M., Hirota T., Hachisuka K., Choi Y. K., Moellenbrock G. A., Bartkiewicz A., 2009, ApJ, 700, 137
Rodriguez-Fernandez N. J., Combes F., 2008, A&A, 489, 115
Roman-Duval J., Jackson J. M., Heyer M., Johnson A., Rathborne J., Shah R., Simon R., 2009, ApJ, 699, 1153
Rygl K. L. J., Brunthaler A., Reid M. J., Menten K. M., van Langevelde H. J., Xu Y., 2010, A&A, 511, A2+
Sanna A., Reid M. J., Moscadelli L., Dame T. M., Menten K. M., Brunthaler A., Zheng X. W., Xu Y., 2009, ApJ, 706, 464
Schutte A. J., van der Walt D. J., Gaylard M. J., MacLeod G. C., 1993, MNRAS, 261, 783
Sevenster M., Saha P., Valls-Gabaud D., Fux R., 1999, MNRAS, 307, 584
Sewilo M., Watson C., Araya E., Churchwell E., Hofner P., Kurtz S., 2004, ApJs, 154, 553
Slysh V. I., Val'tts I. E., Kalenskii S. V., Voronkov M. A., Palagi F., Tofani G., Catarzi M., 1999, A&AS, 134, 115
Solomon P. M., Rivolo A. R., Barrett J., Yahil A., 1987, ApJ, 319, 730
Szymczak M., Bartkiewicz A., Richards A. M. S., 2007, A&A, 468, 617
Szymczak M., Hrynek G., Kus A. J., 2000, A&AS, 143, 269
Taylor J. H., Cordes J. M., 1993, ApJ, 411, 674
van der Walt D. J., Gaylard M. J., MacLeod G. C., 1995, A&AS, 110, 81
van der Walt D. J., Goedhart S., Gaylard M. J., 2009, MNRAS, 398, 961
Vlemmings W. H. T., Goedhart S., Gaylard M. J., 2009, A&A, 500, L9
Voronkov M. A., Caswell J. L., Ellingsen S. P., Sobolev A. M., 2010, 405, 2471
Walsh A. J., Burton M. G., Hyland A. R., Robinson G., 1998, MNRAS, 301, 640
Walsh A. J., Hyland A. R., Robinson G., Burton M. G., 1997, MNRAS, 291, 261
Wilson T. L., Walmsley C. M., Jewell P. R., Snyder L. E., 1984, A&A, 134, L7
Wink J. E., Altenhoff W. J., Mezger P. G., 1982, A&A, 108, 227
van Woerden H., Rougoor G. W., Oort J. H., 1957, Academie des Sciences Paris Comptes Rendus, 244, 1691
Xu Y., Li J. J., Hachisuka K., Pandian J. D., Menten K. M., Henkel C., 2008, A&A, 485, 729
Xu Y., Voronkov M. A., Pandian J. D., Li J. J., Sobolev A. M., Brunthaler A., Ritter B., Menten K. M., 2009, A&A, 507, 1117